SCIENCE REQUIREMENTS DOCUMENT

Microheater Array Boiling Experiment (MABE)

Version 3.1

24 April 2003

Jungho Kim
Principal Investigator
Department of Mechanical Engineering
University of Maryland
College Park, MD 20742

SIGNATURE PAGE
SCIENCE REQUIREMENTS DOCUMENT

Microheater Array Boiling Experiment (MABE)

24 April 2003

Version 3.1

Jungho Kim
Principal Investigator
Department of Mechanical Engineering
University of Maryland
College Park, MD 20742

Signature _____ Date _____

CONCURRENCES:
NASA Lewis Research Center:

John B. McQuillen
Project Scientist
Signature _____ Date _____

Joe Balombin
Project Manager
Signature _____ Date _____

Bhim Singh
Fluid Physics Lead Scientist
Signature _____ Date _____

Fred Kohl
Fluid Physics Program Manager
Signature _____ Date _____

NASA Headquarters:

Fran Chiaramonte
Enterprise Scientist
Signature _____ Date _____

APPROVAL:
Bradley M. Carpenter
Lead Enterprise Scientist
Signature _____ Date _____

TABLE OF CONTENTS

NOMENCLATURE

a	acceleration
A_h	Heater area
AR	Area ratio
Bo	Bond number $\left(= \frac{a(\rho_l - \rho_v)r^2}{\sigma}\right)$
Csf	Surface/fluid coefficient
C_v	Concentration of gas
d_{eq}	equivalent bubble diameter
f	frequency
g	acceleration due to gravity
g_{osc}	amplitude of residual gravity
h_{fg}	Heat of vaporization
H	Henry's constant
k_l	Thermal conductivity of liquid
M	Molecular weight
Ma	Marangoni number
Pr	Prandtl number
P_r	Reduced pressure
P_{sat}	Saturation pressure
P_{tot}	Total pressure
P_v	Vapor pressure
$\dot{q}''$	heat flux
$\dot{q}_h''$	heater heat flux
r	Radius
R_H	Heater Resistance
R_C	Control Resistance
R_P	rms surface roughness
R'	$\sqrt{Bo}$, with Bo based on wire radius
t	time
T_{sat}	Saturation Temperature
T_w	wall temperature
V_{out}	Output Voltage
x	distance
α_l	thermal diffusivity of liquid
λ_c	critical wavelength
λ_D	most dangerous wavelength
μ	dynamic viscosity
ν	kinematic viscosity
ρ_l	liquid density
ρ_g	gas density
ρ_v	vapor density
σ	surface tension
θ	contact angle

LIST OF ACRONYMS

ASCII	text file
CHF	Critical Heat Flux
ISS	International Space Station
LED	Light Emitting Diode
LMS	Life and Microgravity Spacelab
MSG	Microgravity Science Glovebox
NASA	National Aeronautics and Space Administration
NASDA	Japanese Space Agency
NIST	National Institute of Standards and Technology
NSF	National Science Foundation
PGA	Pin Grid Array
RAM	Random Access Memory
TEC	Thermoelectric cooler
TEXUS	Technologische EXperiment Unter Schwerelosigkeit (German Sounding Rocket)
UMD	University of Maryland
VCR	Video Cassette Recorder
VLSI	Very Large Scale Integration

LIST OF FIGURES

LIST OF TABLES

0.0 EXECUTIVE SUMMARY

Boiling as a heat transfer mechanism is of importance to space-based hardware because large amounts of heat can be removed with relatively little increase in temperature. An understanding of microgravity effects on boiling mechanisms is critical to the proper design of heat removal equipment for use in space-based applications. Experiments to date have shown that stable, subcooled pool boiling on flat plates in microgravity environments is possible, although usually with reductions in heat transfer coefficients up to 50% compared with earth gravity values. Relatively little experimental data is available to date regarding the *local* heat transfer rates under and around the bubbles as they grow and depart from the surface. Such data can provide much needed information regarding the relevant wall heat transfer mechanisms during the bubble departure cycle by pinpointing when and where in the cycle large amounts of heat are removed. Microgravity effects on critical heat flux levels is another very important area that must be addressed if boiling is to be used reliably as a heat removal mechanism, and is another area in which little quantitative information is available. By conducting tests in microgravity as well as lunar and martian gravity, it is possible to assess the effect of buoyancy on the overall boiling process and determine the relative magnitude of effects with regards to other "forces" and phenomena such as Marangoni forces, liquid momentum forces, and microlayer evaporation.

The research pertaining to boiling in microgravity environments thus far have been of a qualitative nature (photographic studies) with some wall heat flux/wall temperature measurements, analytical work, or numerical simulations. In the studies where heat transfer coefficients were determined, the heated surfaces were always comparable to or much larger than the bubble sizes, so only heat transfer rates averaged over the entire heated surface were obtained. Very little experimental data is available regarding the *local* heat transfer rates under and around the bubbles as they grow and depart from the surface. Better understanding of the heat transfer mechanisms involved in the boiling process can be attained by pinpointing when and where in the bubble departure cycle large amounts of heat are removed from the wall, and correlating this information to visual observations of the state of the bubble at those times. Such information can provide much needed data regarding the important heat transfer mechanisms during the bubble departure cycle, and can serve as benchmarks to validate many of the analytical and numerical models used to simulate boiling. Improved knowledge of the mechanisms controlling the boiling process will improve the reliability and performance of space-based heat removal equipment.

The objectives of the proposed space experiment are to determine the boiling heat transfer mechanisms in microgravity for two heater sizes at various bulk fluid subcoolings and pressures, and to compare these mechanisms to those at normal, martian, and lunar gravity levels. It is hypothesized that coalescence becomes the primary bubble removal mechanism in microgravity, and causes the formation of a primary bubble. If this bubble is attached to the surface, it causes local dryout to occur, and heat can only be transferred from the surface by the smaller bubbles surrounding the primary bubble. This small-scale boiling behavior is similar across gravity levels, and it is hypothesized that boiling curves in microgravity can be obtained from knowledge of earth gravity data and the size of the primary bubble in microgravity. Measurements will be made from the nucleate boiling regime through CHF and into the transition boiling regime at all test conditions. Numerical and analytical models of the boiling process will be developed and validated using the experimental results.

The proposed experiment uses an array of microheaters to measure the local heat transfer on the surface during boiling. Each heater is on the order of the bubble departure size in normal gravity, but significantly smaller than the bubble departure size in reduced gravity. These heaters are individually controlled to operate at a constant temperature, simplifying the data analysis since the substrate heat conduction can be easily quantified. It also allows one to operate at CHF and into the transition boiling region without danger of heater burnout.

Two experimental packages have been built around the microheater array based on the mechanical design of Prof. Herman Merte's Pool Boiling Experiment. One package was built within a drop tower rack, and flown on the KC-135. Another package was flown on a Terrier Orion Sounding Rocket, and launched in December 1999. Data with the bulk fluid saturated and subcooled have been obtained in earth gravity, microgravity, and high gravity (~1.8 g). Observations to date indicate that microgravity boiling heat transfer is dominated by the formation of a large "primary" bubble on the surface by the coalescence of smaller bubbles. This primary bubble is surrounded by smaller satellite bubbles that rapidly grow and coalesce with the primary bubble. Space-resolved heat transfer measurements indicate that high heat transfer rates are associated with the satellite bubbles. Dryout occurs under the primary bubble, causing CHF in microgravity to be significantly lower than in earth gravity. The primary bubble also limits the size of the smaller satellite bubbles, causing significant bubble activity and higher heat transfer rates. This bubble was also observed to cause nucleation at sites where nucleation would not occur in earth gravity, increasing the heat transfer. Preliminary data indicate that subcooling has a strong effect on the size of the primary bubble and on CHF. The size of the primary bubble increased with lower subcooling and higher wall superheat. CHF increased as the subcooling increased, and occurred at higher superheats. The effect of g-jitter on these measurements is uncertain, however. G-jitter plays an important role as the primary bubble gets larger, and may skew the heat transfer data upward due to occasional detachment of the primary bubble and subsequent rewetting of the surface. Also, the heater size affects the boiling curves. Under certain conditions (low subcooling and/or high wall superheat), the primary bubble was observed to grow large enough to cause dryout over the entire heater array. If the heater array were larger, CHF might be higher and be delayed to higher superheats.

An experimental apparatus for use on the ISS will be developed based on the ground-based experiment hardware. If possible, interferometry will be incorporated into the flight apparatus so temperature contours in the liquid around the primary bubble can be measured. The flight hardware will have two heater array sizes so heater size effects on boiling can be determined.

1.0 INTRODUCTION AND BACKGROUND

1.1 BRIEF OVERVIEW OF SCIENTIFIC TOPIC

Boiling is a complex phenomenon where hydrodynamics, heat transfer, mass transfer, and interfacial phenomena are tightly interwoven. It is of importance to space-based hardware and processes such as heat exchange, cryogenic fuel storage and transportation, electronic cooling, and material processing due to the large amounts of heat that can be removed with relatively little increase in temperature. An understanding of boiling and critical heat flux in microgravity environments is important to the design of future heat removal equipment for these space-based applications. Although much research in this area has been performed since the Space Station was proposed, the mechanisms by which heat is removed from surfaces under these environments are still unclear. It is generally thought that heat is removed from a surface by single bubbles during nucleate boiling is through the following sequence of events. Before bubble initiation, heat is transferred from the wall to the fluid by natural convection (in gravity environments) and heat conduction through the growing thermal boundary layer. Once a bubble forms, various heat transfer mechanisms are possible (see Figure 1.1): conduction heat transfer and natural convection from the heated wall to the fluid ($Q_{\text{liquid conduction}}$ and $Q_{\text{natural convection}}$), conduction through the vapor layer (Q_{vapor}), conduction and evaporation through the microlayer ($Q_{\text{microlayer}}$), evaporation of liquid due to the superheated liquid layer ($Q_{\text{evaporation}}$), and Marangoni (surface tension) convection ($Q_{\text{Marangoni}}$). Of the above mechanisms, it is thought that $Q_{\text{evaporation}}$ and $Q_{\text{microlayer}}$ play dominant roles in the heat transfer process. When the bubble departs from the surface (due to buoyancy forces in gravity or through inertia forces in microgravity), a vortex ring behind the departing bubble is generated which scavenges away the superheated liquid layer and replaces it with a new layer of cold liquid (Han and Griffith–1965). The cycle then repeats. In earth gravity, natural convection and buoyancy are important mechanisms that affect boiling heat transfer through the rate at which bubbles are removed from the surface. A simple model describing the bubble departure size based on a quasistatic balance between buoyancy and surface tension is given by the Fritz (1935) relation:

$$Bo^{1/2} = 0.0208\theta \tag{1}$$

where the contact angle θ is in degrees. For small, rapidly growing bubbles, inertia associated with the induced liquid motion can also cause bubble departure. In microgravity, the magnitude of effects related to natural convection and buoyancy are small and physical mechanisms normally masked by natural convection in earth gravity such as Marangoni convection can substantially influence boiling and vapor bubble dynamics. CHF is also substantially affected by microgravity. In 1-g environments, Bo has been used as a correlating parameter for CHF. Zuber's (1959) CHF model for an infinite horizontal surface assumes that vapor columns formed by the merger of bubbles become unstable due to a Helmholtz instability blocking the supply of liquid to the surface. The jets are spaced λ_D (the Taylor wavelength) apart, where

$$\lambda_D = 2\pi\sqrt{3}\left[\frac{\sigma}{g(\rho_l - \rho_v)}\right]^{1/2} = 2\pi\sqrt{3}L\,Bo^{-1/2} = \sqrt{3}\lambda_c \tag{2}$$

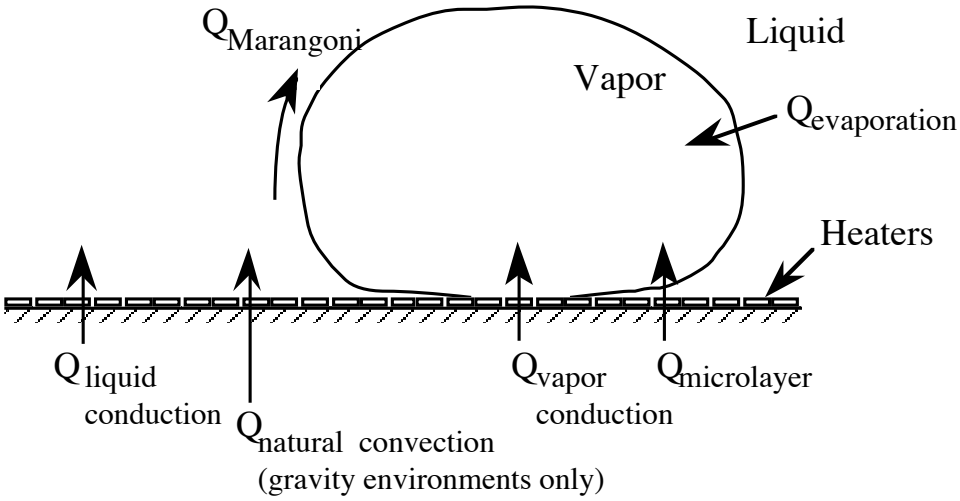

Figure 1.1–Various heat flow paths from a heated wall to a bubble growing above a heated surface.

and is the wavelength that amplifies most rapidly. The critical wavelength, λ_c, is the wavelength below which a vapor layer underneath a liquid layer is stable. For heaters with Bo smaller than about 3 (heaters smaller than λ_D), the above model is not applicable, and surface tension effects dominate. Bubble coalescence is thought to be the mechanism for CHF under these conditions. Small Bo can result by decreasing the size of a heater in earth gravity, or by operating a large heater in a lower gravity environment. In the microgravity of space, even large heaters can have low Bo, and models based on Taylor and Helmholtz instabilities should not be applicable. The macrolayer model of Haramura and Katto (1983) is dimensionally equivalent to Zuber's model, so it should not be applicable as well.

The overarching goal of this work is to determine how boiling heat transfer mechanisms for a flat plate in microgravity are altered from those in earth gravity. It is hypothesized that coalescence becomes the primary bubble removal mechanism in microgravity, and causes the formation of a primary bubble. If this bubble is attached to the surface, it causes local dryout to occur, and heat can only be transferred from the surface by the smaller bubbles surrounding the primary bubble. This small-scale boiling behavior is similar across gravity levels, and it is hypothesized that boiling curves in microgravity can be obtained from knowledge of earth gravity data and the size of the primary bubble in microgravity.

1.2 BRIEF LITERATURE SURVEY

Many of the early experimental studies regarding boiling heat transfer in microgravity environments were first performed under NASA sponsorship in drop towers (See Siegel–1967 and Clark–1968 for a review), and were mainly concerned with determining the effect of gravity on the boiling process. The results of these early experiments were somewhat contradictory, with some experiments showing no effect of gravity on heat transfer and others showing a strong dependence. Much of the discrepancy can be attributed to the relatively short test times that were available since natural convection from before drop initiation could not be eliminated during the short drop time. Visual observations of the boiling process, however, revealed that a

large increase in bubble size (up to a few millimeters) occurred under microgravity conditions, with small bubbles coalescing into larger bubbles a small distance from the heater. Siegel and Keshock (1964), for example, found the bubble departure radius varied approximately as $a^{-1/3}$ for $0.1<a/g<1$, and according to $a^{-1/2}$ for lower gravities.

Straub and co-workers have been looking at boiling in microgravity environments since the early 1980s. (Zell, Straub, and Weinzierl–1984, Vogel and Straub–1990, and Zell, Straub, and Vogel–1989, 1990). Investigations were carried out using sounding rockets (test times of up to 6 minutes) under the TEXUS program, and using NASA's KC-135 aircraft (test times of about 25 s per parabolic flight path). Boiling curves from wires and flat plates at saturated and subcooled conditions were obtained for Freon 12, Freon 113, and water. Their results indicate that gravity has little effect on the overall heat transfer from flat plates, i.e., heater temperatures remained constant for given heat fluxes for $\pm 0.03<a/g<1.8$, although large increases in the bubble departure radius were observed. Bubble departure was felt to occur as a result of the inertia imparted to the surrounding liquid during bubble growth, which subsequently pulled the bubble away from the heated surface. The researchers concluded that buoyancy effects are replaced by surface tension effects (coalescence and evaporation-condensation) in microgravity, so the overall level of heat transfer remains about the same. It was felt by these authors that the primary heat transfer mechanism was evaporation. Nucleate boiling on a small, 1.41 mm diameter hemispherical heater and a 0.02 mm diameter wire was studied by Steinbichler, et al. (1998) on a Spacelab Mission LMS and a Get Away Special using Freon 134a. The results suggest that stable, *saturated* boiling is possible on heaters small compared to the container, in contrast to the findings of Ohta et al. (1997) who found that vapor accumulation near the heater prevented stable, steady-state boiling. They point out that, in contrast to other studies, the dynamics of the vapor generated by their small heaters are not restricted by the test cell. They attribute the high heat transfer coefficients in microgravity saturated boiling to several factors. First, while the nucleation sites on the hemispherical heater and on the wire were concentrated on the top surface of the heater in earth gravity, they were evenly distributed over the entire surface in microgravity. Bubble coalescence and turbulence in the fluid aid vapor removal from the surface. With small subcooling, strong thermocapillary flows were observed to hold the bubbles onto the surface that supported the condensation/transport of vapor from the heated surface to the bulk fluid. With high subcooling, rapid growth and collapse of the bubbles on the surface were observed. Critical heat flux levels were observed to decrease with decreasing gravity, but the use of constant heat flux heaters precluded quantitative measurement of critical heat flux levels with accuracy.

Merte has also performed many experiments in reduced gravity over the years. Lee and Merte (1998) describe the results of boiling experiments using R-113 from five space flights between 1992 and 1996. They used a gold film (19 mm x 38 mm) sputtered on a quartz substrate as both heater and temperature sensor. Boiling behavior for heat fluxes ranging from 2-8 W/cm^2 and subcoolings were obtained. They observed eventual dryout of the surface under high heat fluxes at saturated conditions, but steady nucleate boiling at the same heat flux when the subcooling was increased to 22 °C. When steady nucleate boiling was observed, a very large bubble above the surface acted as a vapor sink for numerous smaller bubbles growing on the heater surface. The large bubble maintained its size due to a balance between condensation at the top of the bubble and coalescence with the smaller bubbles at its base. Enhancements in the heat transfer of up to 32% were observed in microgravity compared to earth gravity. Marangoni convection was also observed to play a significant role in the enhancement of heat transfer since

it caused large vapor bubbles to be impelled toward the heater surface and small bubbles to migrate to the heater surface. Increased subcooling was associated with an increase in heat transfer level. CHF appeared to decrease significantly in microgravity.

Ohta, et al. (1998) measured the heat transfer, local temperature, and local liquid film thickness during boiling of ethanol on a sapphire substrate using a NASDA TR-1A rocket. The local heat transfer was calculated using a numerical simulation of the transient heat conduction within the central 50 mm of the sapphire substrate. The boundary condition information was provided by a row of platinum, thin film temperature sensors deposited directly onto the surface of the substrate. At saturated boiling, a very large bubble on the order of the test vessel size formed above the heater surface, and was "lifted" from the surface by numerous smaller "primary" bubbles. The authors did not observe a macrolayer. Boiling never reached a steady state since the "primary" bubbles grew and collapsed at regular intervals. The high heat transfer was attributed to the extending microlayer and dry spot as the "primary" bubbles grew without a corresponding increase in the dry spot. At high subcooled boiling, small bubbles on the heater surface were observed. Condensation occurred along the top of the bubbles, and steady state boiling was felt to occur.

Dhir, et al. (1998) documented the behavior of single sliding bubbles on downward facing surfaces at various inclinations. A single artificial cavity formed on a polished silicon wafer was used to generate the single bubble. Numerical simulations of the bubble growth and departure were performed at various gravity levels. Experiments on the KC-135 are currently being conducted in preparation for Space Station experiments.

Xu and Kawaji (1998) were perhaps the first to study transition boiling in microgravity. The surface-averaged heat flux and liquid-solid contact frequency were measured with a fast-response, 25.4 mm diameter heat flux gauge built onto a stainless steel plate during a quench with PF-5060. The microgravity environment was obtained using the DC-9. They observed that the frequency of liquid re-wetting in microgravity was significantly lower than that in earth gravity. Vapor film collapse and spreading of the liquid film were thought to be the dominant modes of liquid-solid contact. In earth gravity, both modes are equally significant, but vapor film collapse becomes less significant in microgravity resulting in lower contact frequencies. The heat flux was observed to fluctuate by several hundred kW/m^2 during the quench.

DiMarco and Grassi (1999) studied boiling on a 0.2 mm diameter wire in microgravity using R113 and FC-72 using parabolic aircraft and a sounding rocket. They plotted the enhancement in CHF relative to that of a flat plate vs. R' at various gravity levels for their wire, along with the enhancement at similar R' values obtained for extremely small wires in earth gravity. They found that the microgravity data did not correlate with the earth gravity data, and suggested that separate groups containing the gravity acceleration and wire diameter were needed.

Extremely little work is available regarding the effects of partial gravity on boiling heat transfer. The lack of work by the microgravity boiling community in this area is surprising because data at partial gravity levels can provide insight into the boiling behavior at microgravity as the effect of buoyancy is diminished. Ulucakli and Merte (1990) studied the effects of high-gravity on subcooled boiling, and concluded that the boiling behavior is a complex function of both gravity and subcooling level. Non-boiling natural convection, the activation of nucleation sites, and the heat transfer associated with single nucleation sites all affect boiling heat transfer.

1.3 CURRENT STATUS OF UNDERSTANDING

Experiments to date have shown that stable, subcooled boiling on flat plates in microgravity environments is possible, although usually with some alteration in heat transfer coefficients. It is important to note, however, that all research pertaining to boiling in microgravity environments thus far have been of a qualitative nature (photographic studies) with possibly some wall heat flux/wall temperature measurements, analytical work, or numerical simulations. In the studies where heat transfer coefficients were determined, the heated surfaces were always comparable to or much larger than the bubble sizes, so only heat transfer rates and temperatures averaged over the entire heated surface were obtained. Very little experimental data is available regarding the *local* heat transfer rates under and around the bubbles as they grow and depart from the surface. Better understanding of the heat transfer mechanisms involved in the boiling process can be attained by pinpointing when and where in the bubble departure cycle large amounts of heat are removed from the wall, and correlating this information to visual observations of the state of the bubble at those times. Such information can provide much needed data regarding the important heat transfer mechanisms during the bubble departure cycle, and can serve as benchmarks to validate many of the analytical and numerical models used to simulate boiling. Another technologically important area in which very little research has been performed is the effect of microgravity on critical heat flux. Although it is known that decreasing gravity decreases the critical heat flux level (e.g.–Straub, Zell, and Vogel–1990), relatively little quantitative data is available.

2.0 PI RELATED RESEARCH AND PROPOSED SPACE EXPERIMENT

Development of a technique to measure local values of heat transfer using a microscale heater array held at constant temperatures using electronic feedback loops began under a NASA Research Initiation Award in May, 1994. Much of the development of the heater array and electronic feedback loops was performed under this grant. A second NASA grant was awarded in May, 1996. Documentation of the boiling heat flux behavior from the heater array under earth gravity was performed in March, 1997. A new generation of electronics was then developed that was "faster, better, cheaper". Heat flux measurements in conjunction with high-speed visualization of bubbles during boiling were performed in earth gravity using the new electronics and a high-speed digital video camera. The apparatus was incorporated into a drop-tower rack and flown on the KC-135 to study boiling in microgravity at saturated conditions. A study of single bubble behavior in saturated pool boiling in earth gravity was also performed. In January, 1999, a small grant was awarded to develop a payload that could be flown on the Terrier-Orion sounding rocket. Successful launch of this payload occurred in December, 1999, and data on highly subcooled pool boiling was obtained. A NASA grant was awarded in January, 2000 to perform further ground-based measurements. Studies on the effect of subcooling level on microgravity and partial (martian) gravity pool boiling have been performed under this grant so far. A description of the experimental technique, a summary of results to date, and a statement of the objectives and direction of the proposed research are presented in the following sections.

The microheater array is also being used for other heat transfer studies. NSF awarded a grant in October, 1998 to study transition boiling using a linear heater array. This linear heater array is currently being used by NIST to study heat transfer in microchannels. The Laboratory for Physical Sciences and the Air Force Research Laboratory are jointly sponsoring a study on spray and droplet cooling using the microheater array.

2.1 DESCRIPTION OF EXPERIMENTAL TECHNIQUE

Microscale heater array. Local surface heat flux and temperature measurements are provided by an array of ninety-six platinum resistance heaters deposited on a quartz wafer. A photograph of boiling on this heater array taken through the quartz substrate is shown in Figure 2.1. Each of the individual heaters is about 0.26 mm x 0.26 mm in size, has a nominal resistance of 1000 Ω and a nominal temperature coefficient of resistance of 0.002 $°C^{-1}$. Up to 17 heater arrays can be fabricated simultaneously on a single quartz wafer using VLSI circuit fabrication techniques. Platinum is sputtered onto the entire surface of a 500 μm thick wafer to a thickness of 0.2 μm, a layer of photoresist is deposited and patterned to define the heater geometry, then the platinum from the un-masked areas is removed using an ion mill to form a resistance heater. The platinum lines within each individual heater are 5 μm wide and spaced 5 μm apart. The spacing between each heater in the array varies from 7 μm near the center of the array to typically 40 μm between heaters on the outer edge of the array. Aluminum is then vapor-deposited to a thickness of 1 μm onto the surface, the aluminum power leads are masked off, and the remaining aluminum is removed using a wet chemical etch. A layer of SiO_2 is finally deposited over the heater array to provide the surface with a uniform surface energy. The boiling surface was viewed under an electron microscope, and the surface roughness was found to be on the order of the thickness of the aluminum power leads to the heaters (~1 μm). This dimension is not really significant for boiling nucleation because the critical size of the cavities required to

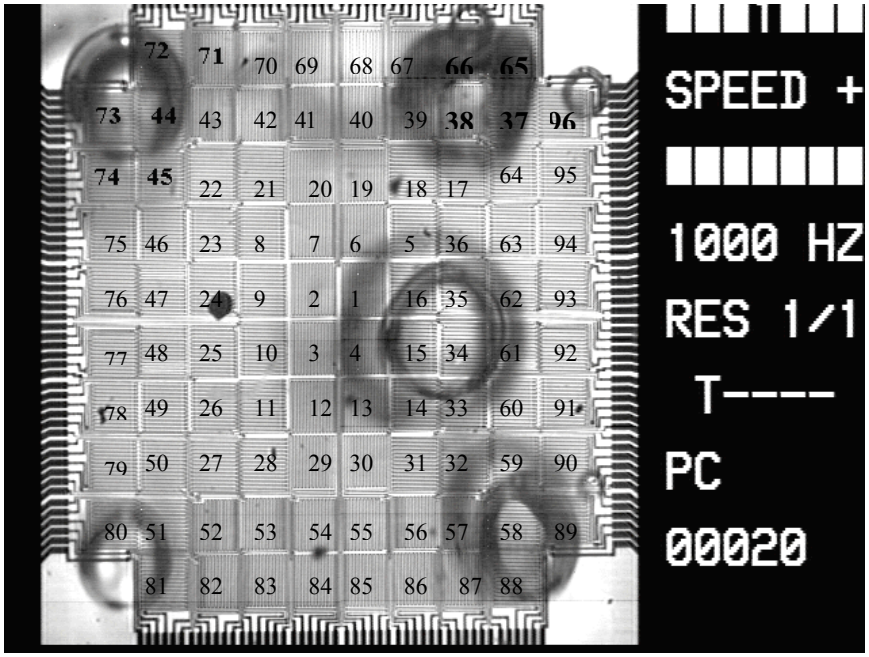

Figure 2.1–Photograph of saturated nucleate boiling taken through the bottom of the heater array in earth gravity. The individual heaters are labeled.

nucleate bubbles is well below 0.1 μm for the highly wetting fluids such as the FC-72 used for this study (Bar-Cohen and Simon–1988). Because the critical cavity size is so small, and because electron microscopes cannot easily resolve such small sizes, it cannot be predicted in advance where nucleation occurs or the size distribution of the cavities.

The completed quartz wafer is diced into chips, each containing a single heater array. The chips are mounted on a pin-grid-array (PGA) package using epoxy adhesive, and the pads on the PGA are connected to the power leads of the heater array chip using a conventional wire-bonding technique. The completed package is then mounted in a PGA socket that is connected to the control and data acquisition apparatus.

Electronic feedback loops. The temperature of each heater in the array is kept constant by feedback circuits similar to those used in constant temperature hot-wire anemometry as shown in Figure 2.2. The op-amp measures the imbalance in the bridge and outputs the necessary voltage to keep the ratio R_H/R_1 equal to R_C/R_2. The temperature of the heater is controlled by changing the wiper position of the digital potentiometer. The instantaneous voltage required to keep each heater at a constant temperature is measured (V_{out}) and used to determine the heat flux from each heater element. The large 200 KΩ resistor at the top of the bridge is used to provide a small trickle current through the heater, and results in a voltage across the heater of about 100 mV even when the op-amp is not regulating. Because all the heaters in the array are at the same temperature, heat conduction between adjacent heaters is negligible. There is conduction from each heater element to the surrounding quartz substrate (and ultimately to the walls of the chamber where it was dissipated by natural convection), but this can be measured and subtracted from the total power supplied to the heater element, enabling the heat transfer from the wall to the fluid to be determined.

The frequency response of the heaters along with the control circuit was found to be 15 kHz by measuring the time it took for the voltage across a heater to stabilize after a step change

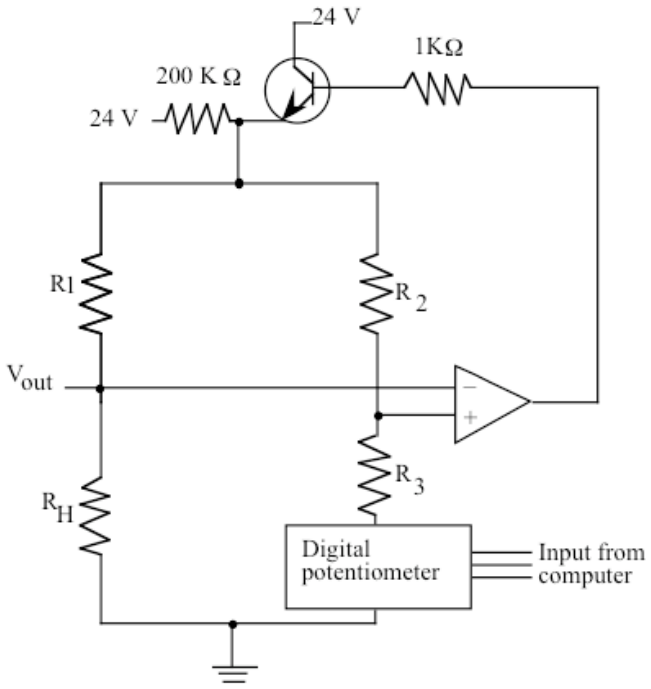

Figure 2.2–Schematic diagram of feedback control circuit.

in the digital potentiometer position. Because this is much faster than the time scales typically associated with pool boiling, the heater temperatures are essentially constant throughout the bubble departure cycle.

2.2 EXPERIMENTS: 1G LABORATORIES, AIRCRAFT, AND SOUNDING ROCKET

We have been conducting experiments in earth and microgravity using a microscale heater array to measure time and space-resolved heat transfer, and have started to address some of the questions associated with microgravity boiling. The fluid is FC-72 at 1 atm. Measurements were performed in normal gravity at saturated conditions from nucleate boiling, through CHF, and into the transition boiling region (Rule and Kim-1999). Measurements underneath bubbles generated from a single nucleation site at two wall superheats have also been made to determine how heat is transferred by individual bubbles (Yaddanapuddi and Kim-2001, Kim, Demiray and Yaddanapuddi-2000). Measurements were made in microgravity environments provided by the KC-135 at saturated and subcooled conditions (Kim, Yaddanapuddi, and Mullen-2001, Kim, Benton, and Kucner-2000, Kim and Benton-2001). Finally, measurements with a highly subcooled bulk liquid were made using the Terrier-Orion sounding rocket (Kim and Benton,-2001), and subsequently in the KC-135 at other subcoolings. The results of these investigations are reviewed below.

A schematic of the experimental apparatus used in the ground-based experiments is shown in Figure 2.3. This apparatus was supplied by NASA, and is a prototype for Merte's

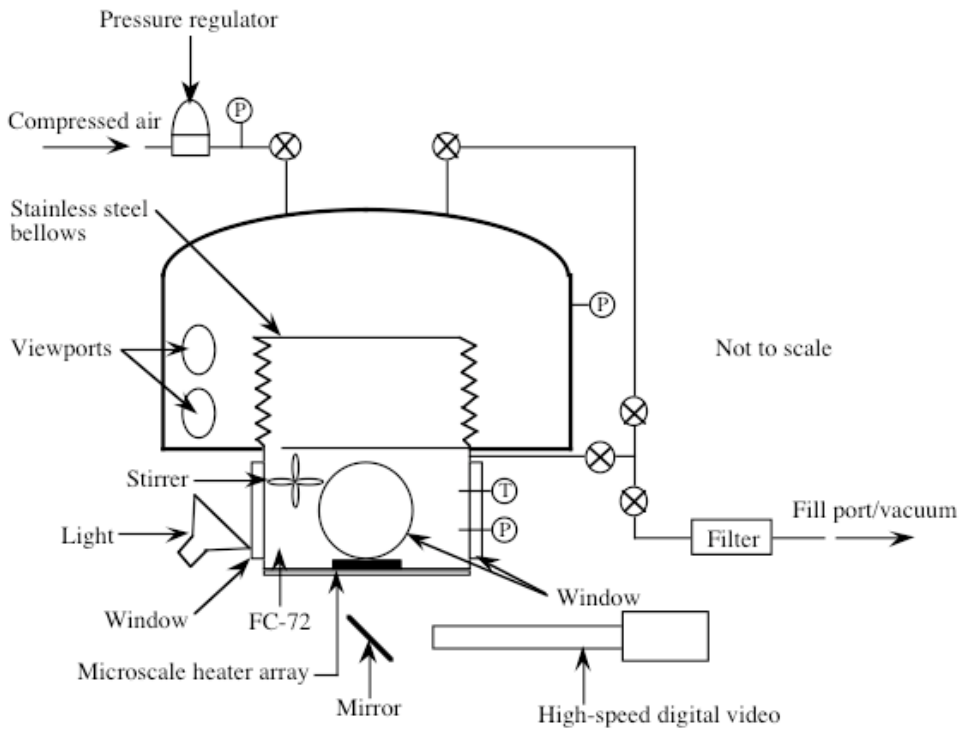

Figure 2.3: Functional schematic of the boiling chamber.

space shuttle experiments. The bellows and its surrounding housing allow the test section pressure to be controlled. A stirrer is used to break up stratification within the test chamber, and a temperature controller and a series of Kapton heaters attached to the boiling chamber are used to control the bulk fluid temperature. Detailed description of the experimental apparatus and the heater array is given in Rule, et al. (1999) and Rule (1997). A similar apparatus was used in the sounding rocket experiment, but without the stirrer and high-speed digital video camera.

Earth gravity, saturated bulk liquid. Saturated boiling on the heater array in the nucleate, CHF, and transition boiling regimes was documented in Rule and Kim (1999). Space-resolved heat transfer measurements indicated that heaters towards the center of the array reached critical heat flux at significantly lower wall superheats (~30 °C) than the array averaged heat flux (~35 °C) due to the edge heaters blocking the flow of liquid to the inner heaters. Obtaining data at critical heat flux and during transition boiling was not a problem since the heaters were operated in constant temperature mode. It was also possible to distinguish regions on the heater that were covered with vapor from those where liquid contact occurred in transition boiling by using the time-resolved data from each heater to deduce a *boiling function*, a bi-modal signal that goes HIGH when boiling occurs on the surface. An example of a time-resolved signal in the transition boiling regime along with the corresponding boiling function is shown on Figure 2.4. The *boiling fraction* is defined as the time average of the boiling function, and represents the time fraction that boiling or enhanced convection occurs on the surface. Within transition boiling, where the surface is alternately wetted by liquid and vapor, the boiling fraction is equivalent to (1-void fraction), or the liquid fraction). The heat transfer from the edge heaters were observed to be much higher than those for the inner heaters above the temperature corresponding to CHF. The heat transfer during liquid contact in transition boiling was constant

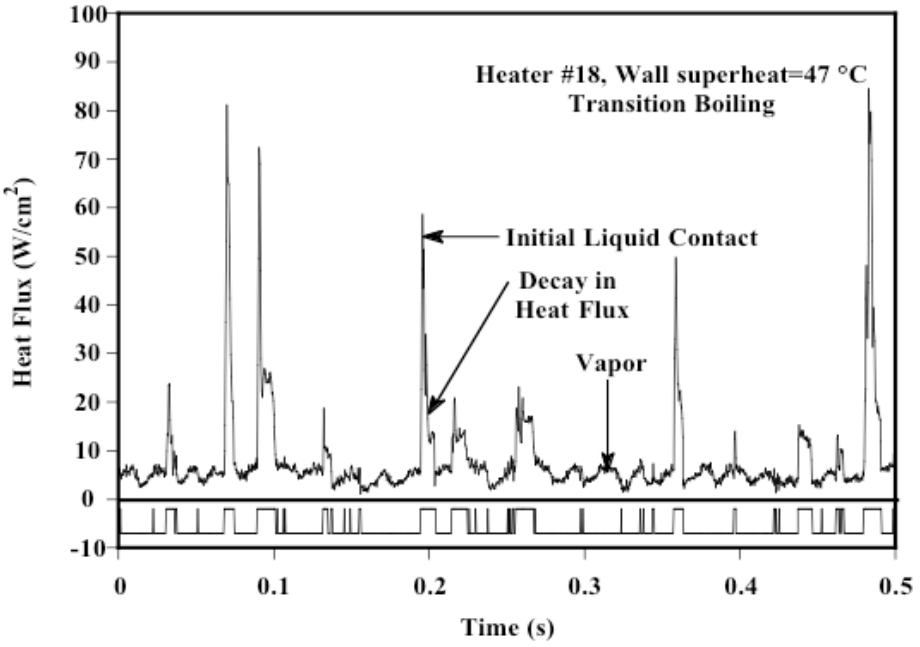

Figure 2.4: Time-resolved signal with the corresponding boiling function for a single heater in the array (from Rule and Kim, 1999).). See Fig. 2.1 for heater numbering.

for a given wall superheat for the inner heaters, and was observed to decrease with increasing wall superheat.

The behavior of bubbles growing from a single nucleation site on the array was studied in Yaddanapudi and Kim (2000) and Kim, Demiray, and Yaddanapudi (2000). The state of the bubbles were visually recorded along with the wall heat flux as they grew and departed from the surface at wall superheats of 22.5 °C and 27.5 °C. The bubbles that nucleated at this site alternated between two modes: chaotic bubble departure and periodic bubble departure. During chaotic bubble departure, bubble nucleation was observed immediately after the previous bubble departed, with the departing bubble pulling the growing bubble off the surface prematurely. During periodic bubble departure, the bubbles departed the surface at very regular intervals. What caused the bubble behavior to alternate between the two is currently not known.

A plot of the wall heat transfer with time during periodic bubble departure for the 22.5 °C superheat case is shown on Figure 2.5. Time t=0 corresponds to nucleation for each bubble. It is seen that the wall heat transfer during bubble departure associated with all seven bubbles are quite repeatable. A sharp increase in heat transfer is associated with the initial growth of the bubble, and is most likely associated with microlayer evaporation during the time the bubble grows hemispherically due to the rapid growth of the bubble. The heat transfer then decreases, perhaps as the microlayer dries out, then increases again as the dry spot shrinks and liquid rewets the surface. A decay in heat transfer back to the baseline occurs after bubble departure.

The wall heat transfer data shown can be used to compute an equivalent bubble diameter (d_{eq}) assuming that all the heat transferred from the wall goes into latent heat:

$$\rho_v \frac{\pi d_{eq}^3(t)}{6} h_{fg} = \int_0^t \dot{q}_h''(t) A_h \, dt \Rightarrow d_{eq}(t) = \sqrt[3]{\frac{6}{\pi \rho_v h_{fg}} \int_0^t \dot{q}_h''(t) A_h \, dt} \tag{3}$$

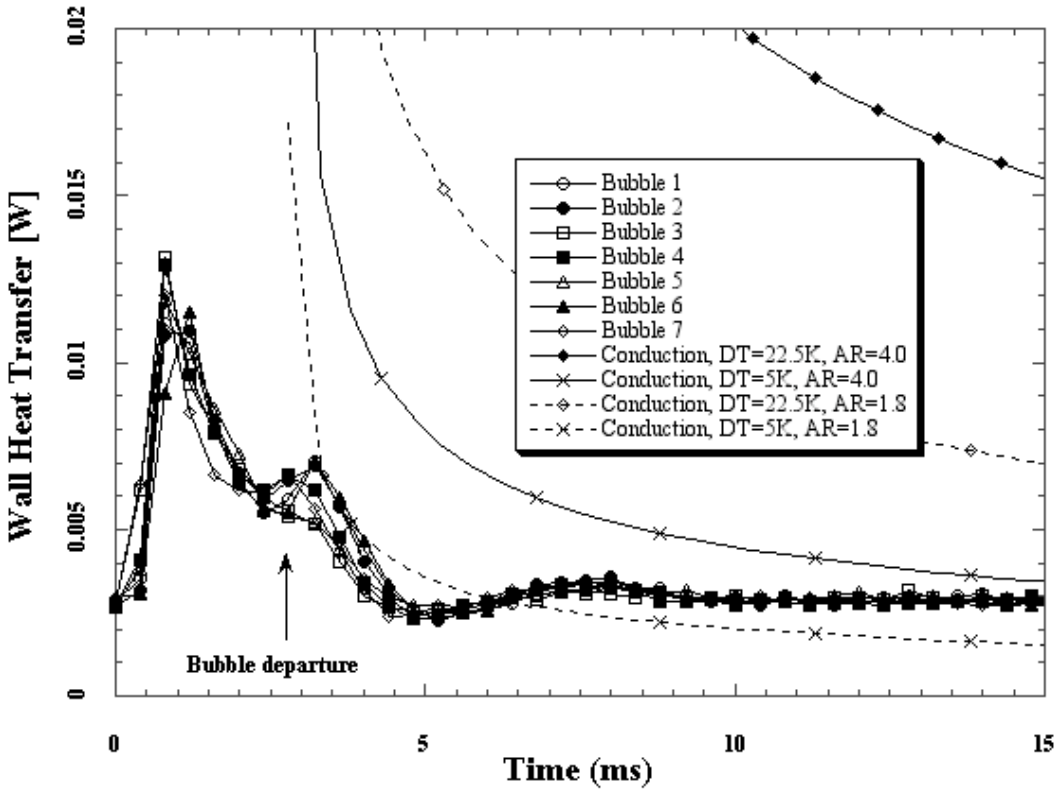

Figure 2.5: Heat flux vs. time for seven bubbles in the periodic regime.

where $\ddot{q}_h(t)A_h$ is the heat transfer from heater [W]. d_{eq} for two bubbles from nucleation to bubble departure is shown on Figure 2.6 along with measured bubble diameters. The size of the uncertainty bars is due to the uncertainty in the magnitude of the baseline heat transfer. It is seen that d_{eq} is significantly lower than the measured bubble diameter during the bubble growth time, indicating that the bubble gains the majority of its energy from the superheated liquid surrounding the bubble and not from the wall.

The value for d_{eq} at the end of the bubble cycle time (just before the next bubble nucleates) is 0.47 mm. The fraction of total energy transferred from the wall that is manifested as latent heat can be computed to be approximately 49%. Because of the uncertainty in the baseline heat transfer level, which builds up over the bubble departure cycle, this could be as small as 26% or as high as 62%. It is important to note, however, that much of this latent heat comes from the energy that was stored in the superheated layer during the waiting time, and not through microlayer evaporation or evaporation of liquid at the bubble base. The remaining energy is transferred by microconvection/conduction. These results indicate that microlayer evaporation does not play a significant role in bubble growth or boiling heat transfer in the periodic bubble regime. The transient conduction model of Mikic and Rosenhow (1969) is much more consistent with the observed behavior.

A popular method to model bubble heat transfer is to assume that the bubble scavenges away the superheated layer surrounding the bubble over some area of influence as it departs, allowing cold liquid at T_{sat} to contact the surface. The superheated layer is renewed during the waiting time by transient conduction into the liquid. The heat transfer during this time is given by

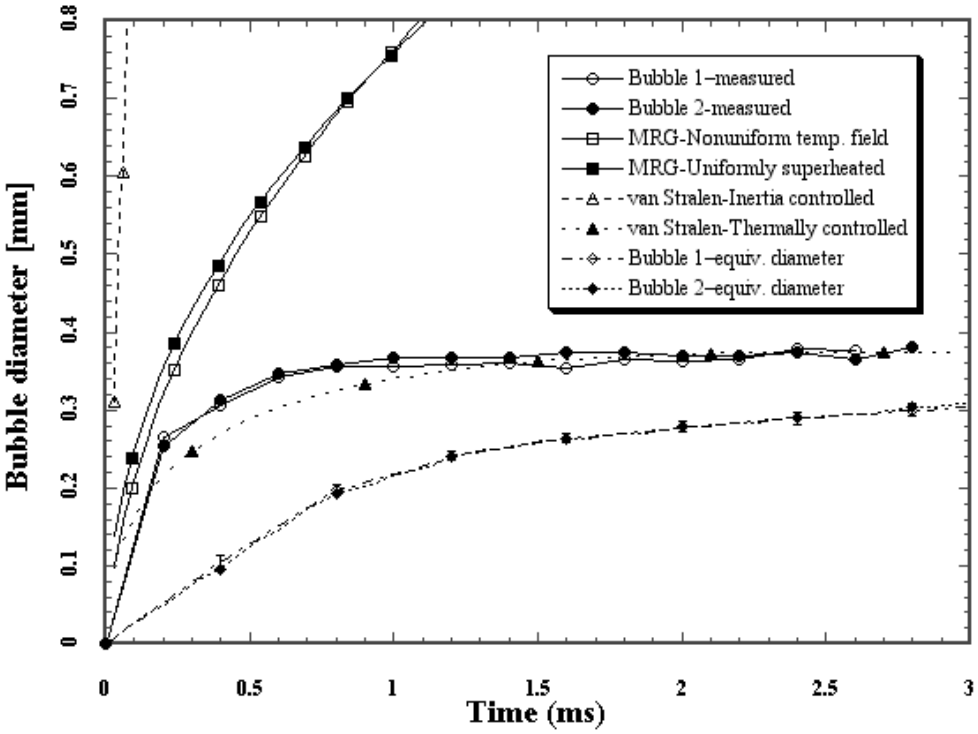

Figure 2.6: Measure bubble diameter and equivalent bubble diameter vs. time.

$$\dot{q}'' = \frac{k_l(T_w - T_{sat})}{\sqrt{\pi \alpha_l t}} \quad \left[W/m^2\right] \tag{4}$$

To evaluate this model, the transient conduction heat transfer was computed assuming various areas of influence and wall to fluid temperature differences, as shown on Figure 2.5. Liquid was assumed to come into contact with the wall about 0.4 ms before the bubble vapor stem separated from the surface. The area of influence is given as an area ratio:

$$\text{AR} = \frac{\text{Area of Influence}}{\text{Bubble Projected Area at Departure}} \tag{5}$$

Mikic and Rosenhow (1969) proposed AR=4 based on experiments with a sphere that was suddenly pulled away from the bottom of a tank, while Koffman and Plessett (1983) found AR=1.8 best fit their data.

The transient conduction model of Mikic and Rosenhnow (1969) is seen to greatly overpredict the wall heat transfer even for AR=1.8. It may not seem possible that the wall heat transfer can be lower than that for transient conduction since any convection that exists should *increase* the wall heat transfer above that for transient conduction. However, it is possible that the liquid coming into contact with the wall after bubble departure is not from the bulk but from the superheated layer in the vicinity of the bubble. If so, then the fluid would be significantly warmer than the bulk temperature and the wall heat transfer would decrease. Significant motion of liquid parallel to the wall in the vicinity of a growing and departing bubble was observed by Nakayama and Kano (1992) using solid tracer lycopodium spores. AR has the same influence as

temperature difference on transient conduction. It is seen on Figure 2.5 that the decay in heat transfer after bubble departure could possibly be explained by transient conduction if the fluid coming into contact with the wall is close to the wall temperature (DT=5 K and AR=1.0 case). Because the area of influence is not known, however, it is not possible to determine what this fluid temperature is. Similar results were observed for a wall superheat of 27.5 °C in the periodic regime (Kim, Demiray, and Yaddanapuddi-2000).

Microgravity, saturated bulk liquid. The test apparatus was incorporated into a drop tower rack and flown on the KC-135 four separate days in August, 1998, to obtain data at saturated conditions. Pictures of the boiling process were obtained using a 30 Hz video camera. The package was flown both mounted to the floor and as a free-float package. Space and time-resolved heat flux maps were obtained and correlated with video images of boiling recorded through the heater surface. The time-resolved heat flux data were conditionally sampled according to whether or not boiling occurred on the surface and an average heat flux during boiling was obtained. Some preliminary observations and data are summarized below.

Array averaged boiling curves in earth and microgravity are shown in Figure 2.7. It is seen that heat fluxes in microgravity are slightly larger than in earth gravity for wall superheats up to about 30°C, but are significantly lower than in earth gravity at higher superheats. CHF in microgravity is about 30% of the value in earth gravity. The heat flux conditionally sampled on boiling, however, was independent of the gravity condition (Figure 2.8) suggesting that the small-scale bubble behavior is not affected by gravity. Heat transfer from the surface occurred primarily through these small bubbles, and not much heat transfer was associated with the large bubble that occasionally formed on the surface as a result of coalescence of the small bubbles. Additional details are given in Kim, Yaddanapudddi and Mullen (2001).

The data obtained were complicated by g-jitter, however. The large bubble that formed on the surface occasionally moved off the surface due to g-jitter, resulting in artificially high values of wall heat transfer at higher wall superheats as liquid flowed in behind the bubble. It is also thought that a single bubble eventually forms that covers the entire heater under saturated conditions, but this was not observed at lower superheats during the microgravity times provided by the KC-135. At high superheats, bubbles are generated from the surface very quickly and these bubbles rapidly coalesce to form a primary bubble. At low superheats, the large g-jitter on the aircraft may have hindered formation of a primary bubble since the individual bubbles grow more slowly and may be pulled off the surface before coalescing.

Microgravity, highly subcooled bulk liquid. The experiment test rig was repackaged for a Terrier-Orion sounding rocket between January, 1999 and September, 1999. Launch of the sounding rocket from Wallops Island occurred on December 17, 1999, and 200 seconds of very high quality microgravity (10^{-6} g) with a maximum roll rate of 0.2 °/s was achieved in all three axes. Data was taken with the fluid at 1 atm (T_{sat}=56 °C) and a subcooling of 36 °C at a frequency of 250 Hz/heater. The first point in the matrix was a nucleation run where the heater temperature was set to about 110 °C in order to start nucleation. The heater temperature was then decreased from 85 °C down to 65 °C in 5 °C increments. Data was collected for 25 seconds at each temperature. The sequence from 85 °C down to 65 °C was then repeated.

Data from the flash disk was successfully recovered from the payload, but it was found that the VCR did not record. In order to obtain additional data including video data, the experiment payload was repackaged to fly on the KC-135. This package was flown in late April,

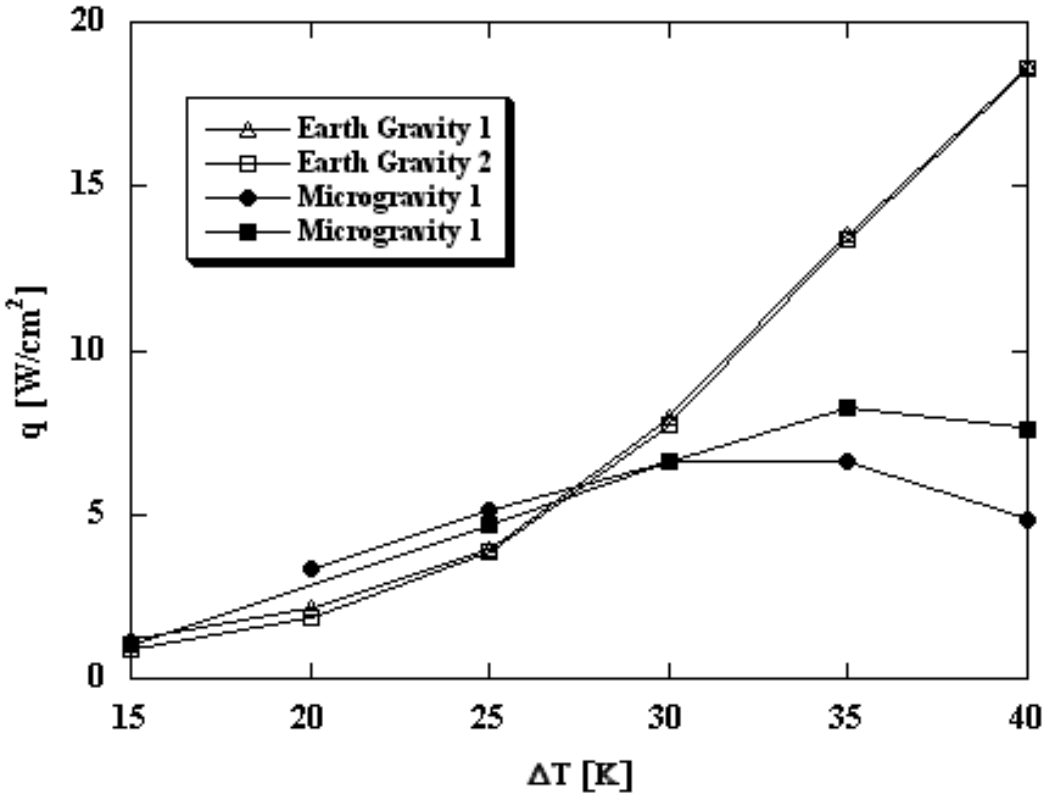

Figure 2.7: Boiling curves in earth and microgravity, saturated conditions.

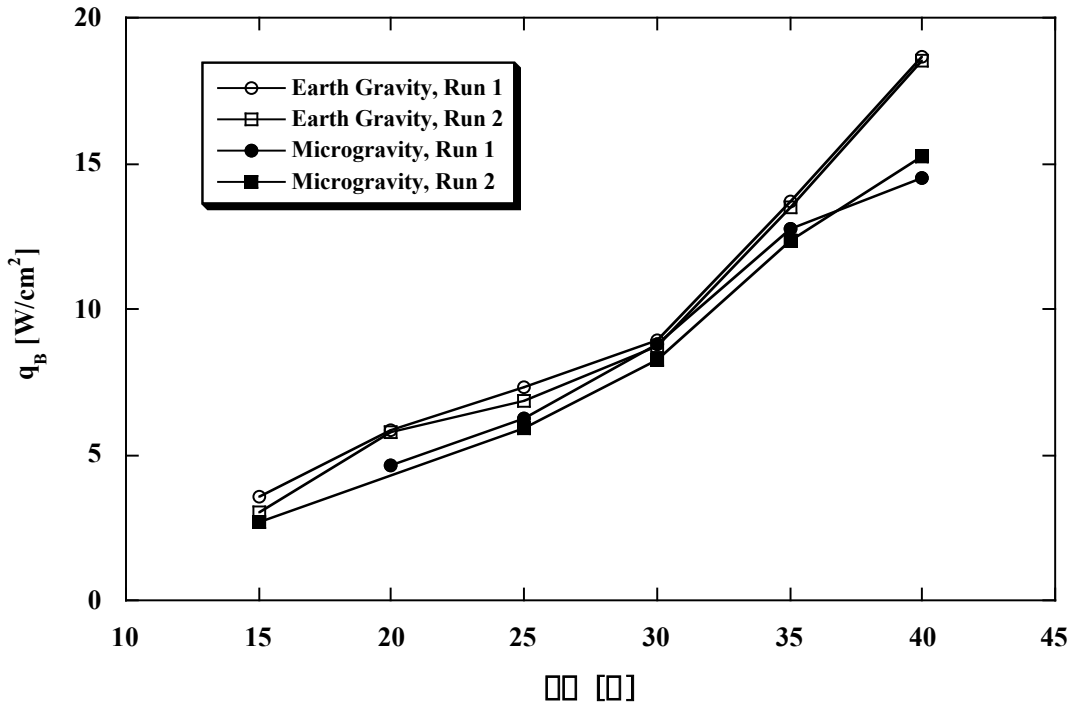

Figure 2.8: Boiling heat flux, saturated conditions.

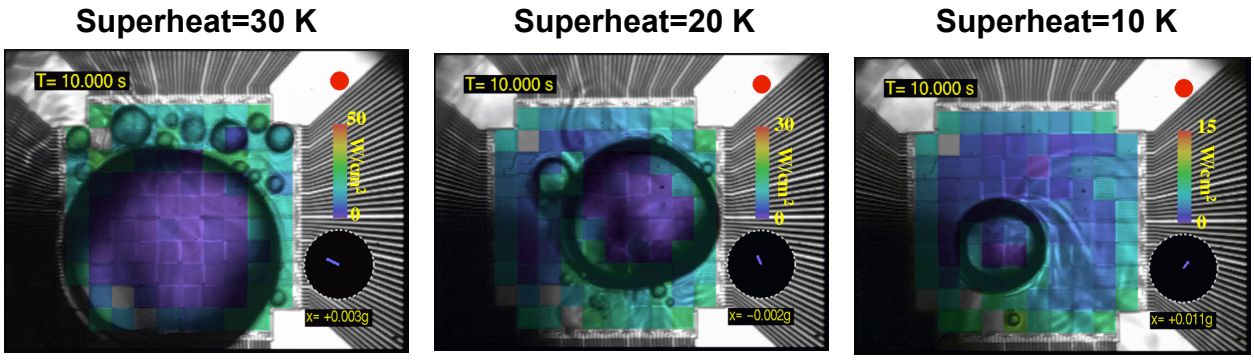

Figure 2.9: Space-resolved heat transfer distributions on the array in microgravity.

2000. The same heater array used in the sounding rocket flight was used during the aircraft tests in order to minimize variation in heat transfer due to different nucleation site distributions. Use of the KC-135 allowed data to be obtained at high-g levels as well. Additional earth gravity data was taken after the KC-135 flights were completed.

The data indicated that there is little effect of gravity on boiling heat transfer at wall superheats below 25 °C, although there are vast differences in bubble behavior between gravity levels. At all superheats in microgravity, a relatively large primary bubble moved over the surface, occasionally causing nucleation of new bubbles to occur. This primary bubble was surrounded by smaller satellite bubbles that eventually merged with the primary bubble. This primary bubble initially forms by the coalescence of smaller bubbles generated on the surface, but then remains constant in size for a given superheat, indicating a balance between evaporation at the bubble base and condensation along the bubble interface. The size of the primary bubble increased with increasing wall superheat. Most of the heaters under the primary bubble indicated low heat transfer, indicating that dryout occurred on the heater surface. High heat transfer was associated with the three-phase contact line and the area surrounding the primary bubble where nucleate boiling occurred. Strong Marangoni convection around the bubble developed in microgravity, forming a "liquid jet" of fluid into the bulk fluid. This "jet" provided a reaction force on the primary bubble, helping to keep the bubble on the heater. At a superheat of 30 °C, the microgravity heat flux fell significantly below the 1 g and 1.8 g data due to a large part of the heater surface drying out.

Space-resolved heat transfer distributions on the array at three superheats are shown on Figure 2.9, where each heater has been color-coded according to the heat transfer. Low heat transfer is associated with the dry area underneath the primary bubble, while large amounts of heat transfer occur during satellite bubble growth and departure and on the heaters cooled by convection. Occasionally, a satellite bubble grew large enough that the dry area underneath it became larger than a single heater, causing the heat flux from that heater to drop to a low value.

Boiling curves were generated from data taken on the sounding rocket, the KC-135, and in earth gravity. The KC-135 data was split into microgravity and high-g data, with separate curves being generated for each. Comparison of this data with microgravity and earth gravity data taken at saturated conditions using a different heater array and test rig (see Kim, et al.—2000) is shown on Figure 2.10. The uncertainty in the heat flux is about 2 W/cm^2.

Significant differences between earth gravity, high-g, and microgravity data are observed. First, all of the subcooled heat fluxes are significantly higher than those for saturated conditions due to the increase in the natural convection heat transfer. Part of the difference in heat fluxes

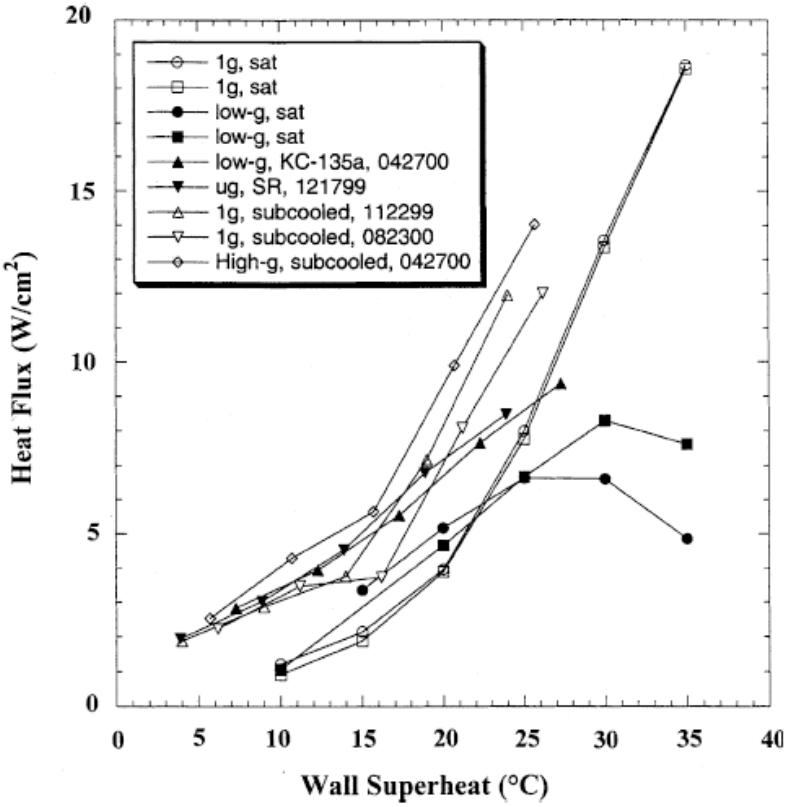

Figure 2.10: Boiling curves in earth and microgravity at saturated and subcooled conditions.

could, however, be due to different nucleation site density distributions since another heater array was used to take the saturated and subcooled data. The differences are slight, and the uncertainty in the data makes it uncertain whether or not there is a real shift between the two curves.

Second, earth gravity heat fluxes are seen to be slightly lower than both the microgravity and high-g data taken on the KC-135 at superheats below 25 °C, but still within the uncertainty band. The sounding rocket data falls between the two. It should be noted that the earth gravity data taken before the sounding rocket was launched and after the KC-135 data was taken (almost eight months apart) agree, indicating that both the heater array and control electronics were stable throughout the test program. Calibration of the heater array before the sounding rocket launch and after the KC-135 tests were completed also revealed very little shift in the calibration, further indicating that the electronics and heater array were stable.

Third, the microgravity data and high-g data taken in the KC-135 are seen to agree with each other for wall superheats below 25 K, despite the large difference in bubble behavior on the surface.

Fourth, the microgravity heat fluxes at the highest wall superheat (30 °C) fall below those for earth gravity and high-g environments due to the primary bubble covering a large portion of the heater in microgravity. Boiling curves obtained from those areas of the heater on which boiling occurred (i.e., the heaters are ignored when only natural convection occurs on the heater, or if the heater goes dry due to the primary bubble), however, were found to be quite independent of the gravity level even at the highest wall superheat (Figure 2.11), indicating that the small-scale bubble heat transfer is independent of the gravity level. This suggests that if one

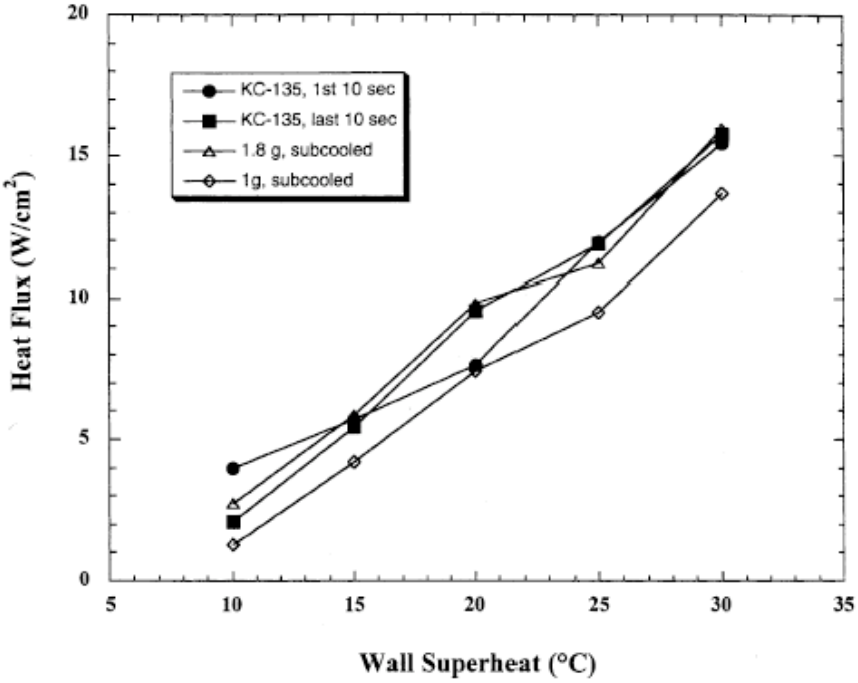

Figure 2.11: Boiling heat flux in microgravity, earth gravity, and high-g.

is able to predict the extent of the dry area in microgravity, then one should be able to predict the microgravity boiling curve from earth gravity boiling heat flux data.

The boiling curves are consistent with the observations of Merte et al. (1998) who observed higher heat transfer in microgravity than earth gravity at low superheats, but significantly lower critical heat fluxes in microgravity. They also observed increases in heat transfer in microgravity as subcooling increased.

Microgravity, effect of subcooling. Additional data was obtained on the KC-135 in January, 2001, and again in May, 2001. In both these series of flights, the bulk liquid temperature was varied from 20 °C to 50 °C (subcooling from 36 °C to 6 °C), and measurements were made to much higher wall superheats. A summary of the test conditions is given on Table 2.1. Analysis of this data set is not complete, so the following results should be considered preliminary. Single frames from the high-speed video over the entire range of test conditions obtained through the bottom of the heater are shown on Figure 2.12. A large primary bubble is seen to form whose size is on the order of the heater array. This bubble formed from the coalescence of smaller bubbles that grew on the surface after transition into microgravity. The primary bubble increases in size with increasing bulk fluid temperature and wall superheat, and is fed by smaller satellite bubbles that surrounded it. For a given bulk temperature, the size of the satellite bubbles decreases with increasing superheat since the size to which they are able to grow is limited by the increasing size of the primary bubble. The satellite bubbles themselves were surrounded by even smaller bubbles which fed them, resulting in an almost fractal pattern to the boiling process. This suggests an approach to modeling low Bo boiling (boiling in microgravity or on small heaters in earth gravity) where a large primary bubble forms that is fed by smaller bubbles, which in turn are fed by even smaller bubbles. Larger heaters would simply have a primary bubble with a larger length scale. The formation of a primary bubble similar in size to the heater surrounded by satellite bubbles of a range of sizes were observed in videos of

Flight No.	T_{bulk} (°C)	Saturation Temperature (°C) [Subcooling level (°C)]		
		Microgravity	High-g	1-g
1	39.5	59.5 [20.0]	61.2 [21.7]	61.2 [21.7]
2	49.6	56.6 [7.0]	57.9 [8.3]	58.2 [8.6]
3	30.9	56.3 [25.4]	57.6 [26.7]	57.8 [26.9]
4	23.0	55.6 [32.6]	56.9 [33.9]	56.9 [33.9]

Table 2.1: Summary of test conditions for each flight. The saturation temperatures for each g-level were calculated based on the measured average liquid pressure and the thermodynamic data provided by 3M.

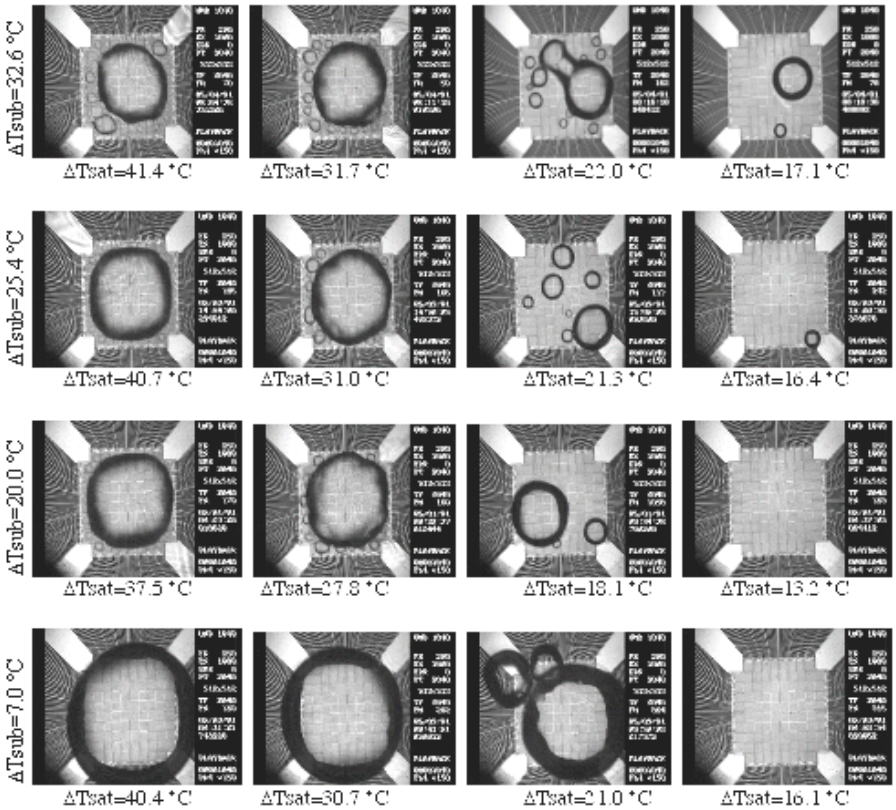

Figure 2.12: Pictures of the bubble from below.

microgravity boiling taken by Merte and Chiaramonte (2001) on a rectangular heater 19.1 mm x 38.1 mm.

The motion of the primary bubble at low bulk temperatures was less influenced by g-jitter, since they were smaller and moved about the surface due to coalescence with the satellite bubbles. The size of the primary bubble is determined by a balance between vapor addition by evaporation of liquid at the bubble base and coalescence with satellite bubbles, and heat loss by condensation through the bubble cap.

Side-view images at selected conditions are shown on Figure 2.13. Strong Marangoni convection around the bubble was observed to develop, forming a "jet" of liquid into the bulk liquid. This "jet" also provided a reaction force on the primary bubble, keeping it on the heater. Partial dryout under the primary bubble occurred for bulk temperatures 39.5 °C and below. Dryout for the edge heaters did not occur, probably due to the flow induced by the Marangoni convection. Dryout over the entire heater array occurred for T_{bulk}=49.6 °C at superheats above 30.7 °C–dryout might have occurred as low as 25.7 °C, but g-jitter caused the primary bubble to move slightly off the heater array, enabling liquid to rewet the edges of the heater. The contact line of the bubble was stable, and touched the outside of the heater array. Bubble coalescence seemed to be the mechanism by which CHF occurred under the conditions studied. No evidence of Taylor instability was observed at any of the test conditions. This is not surprising since the heater array size is much smaller than λ_D (about 8 mm under the conditions studied).

Boiling curves for microgravity, earth gravity, and high-g for various subcoolings are shown on Figure 2.14. The high-g boiling curve is based on the middle 20 s of the high-g data, and includes data from the pull out (~1.6 g) and pull up (~1.8 g). Separate boiling curves were generated from the data taken during the pull out and compared with those during the pull up, but little difference in the curves was observed. The microgravity curves are an average of all the data obtained during the first and second microgravity periods. The effect of g-jitter must be considered for the microgravity curves. Higher wall superheat is generally associated with larger primary bubbles, which are more sensitive to g-jitter. When the primary bubble moves on the surface or departs due to g-jitter, liquid rewets the surface and results in higher wall heat transfer than would occur in a true microgravity environment. The data at high bulk temperatures and high wall superheats (especially those beyond CHF) may be artificially high as a result.

Little effect of subcooling is seen in the nucleate boiling regime for the 1 g and high-g data, which is consistent with the observations of previous researchers. The microgravity data tend to follow the 1 g and high-g data for ΔT_{sat}<20 °C, but drop below them for higher superheats as the primary bubble causes dryout over a successively larger fraction of the heater. CHF for the microgravity curves are significantly lower than that for the 1 g and high-g data.

A plot of CHF vs. gravity and bulk fluid temperature is shown on Figure 2.15. CHF is observed to increase with gravity and subcooling. The percentage increase in CHF, however, increases as the bulk temperature increases and as the gravity level decreases. Increased subcooling is seen to increase CHF dramatically, and there seems to be an increase in the wall temperature at which CHF occurs. Similar observations were made by Merte, et al. (1998). Heater size effects on CHF under these conditions is not known. Experiments to address this are planned in the future. Kutateladze (1952) postulated that CHF in subcooled boiling should be increased above that required for saturated conditions by the amount of energy required to bring the subcooled liquid up to saturated conditions. He proposed a correlation of the form:

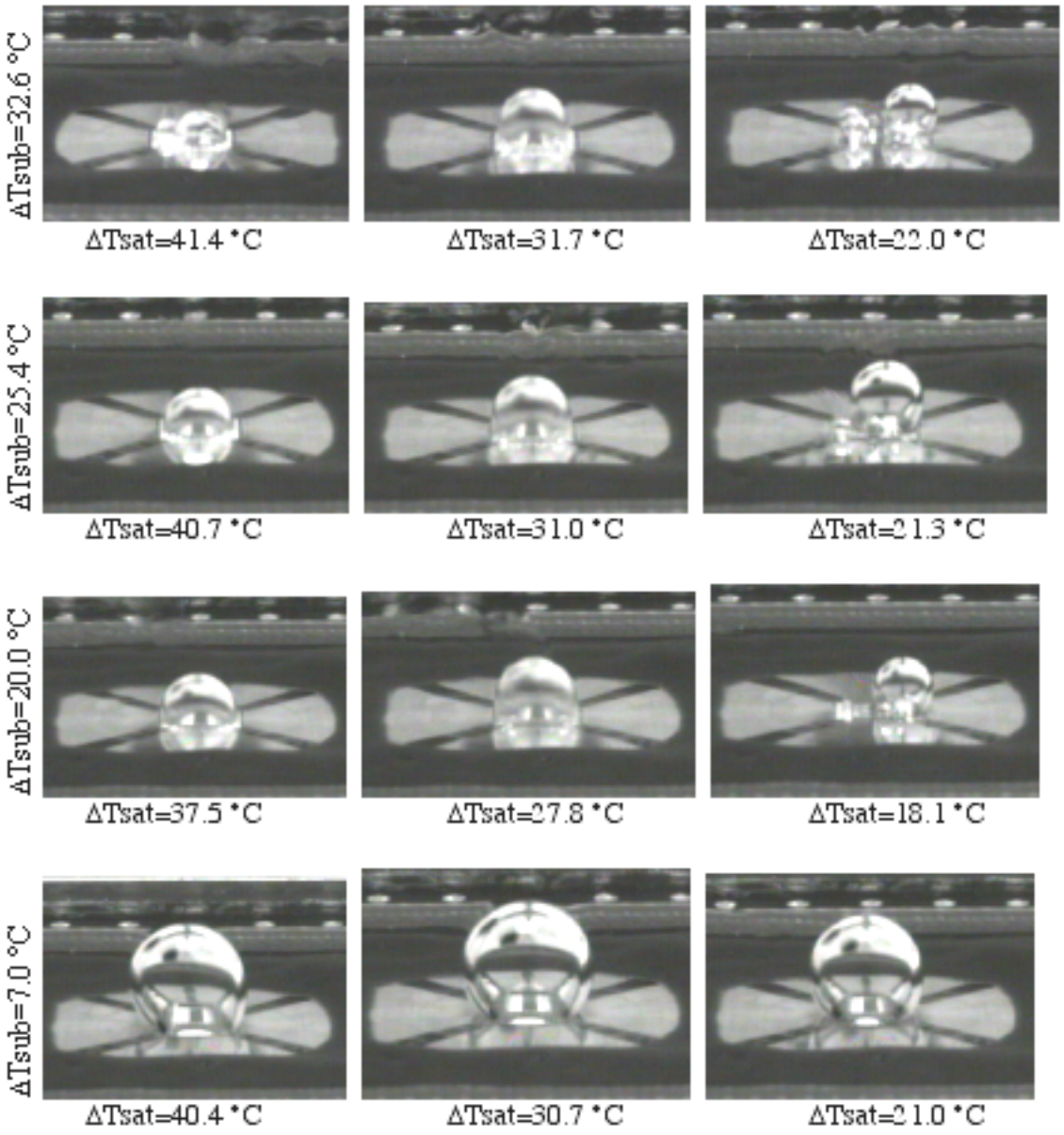

Figure 2.13: Pictures of bubbles from the side.

$$\frac{\dot{q}''_{CHF,sub}}{\dot{q}''_{CHF,sat}} = 1 + C_o\left(\frac{\rho_l}{\rho_v}\right)^m \frac{c_{pl}(T_{sat} - T_l)}{h_{fg}} \tag{6}$$

Ivey and Morris (1962) suggested C_0=0.1 and m=0.75 based on available data. The above correlation indicates that gravity does not affect the enhancement in CHF. Using this correlation to normalize the CHF data in Figure 2.15 those at T_{bulk}=49.6 °C according to

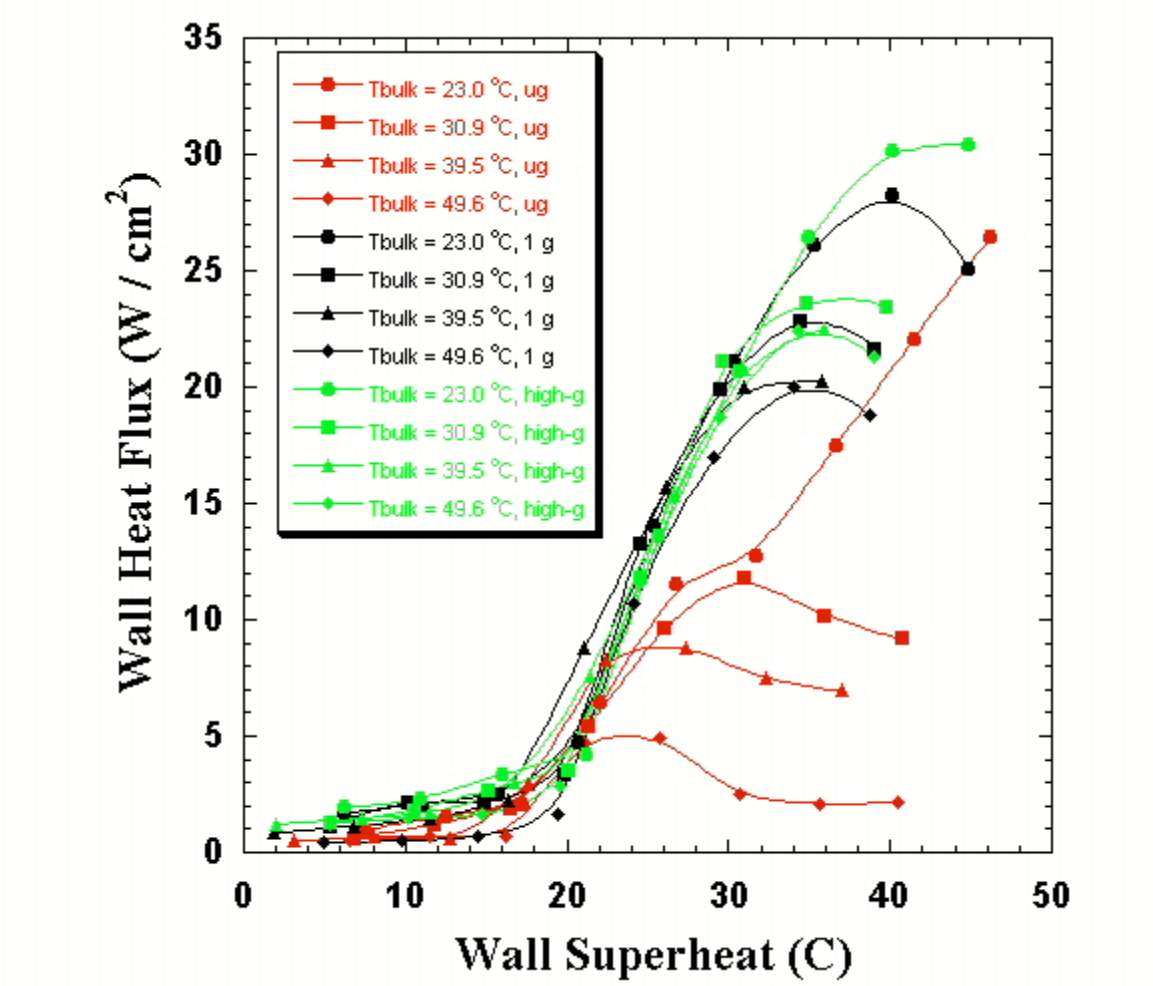

Figure 2.14: Boiling curves showing the effect of subcooling on boiling at three gravity levels.

$$\frac{\dot{q}''_{CHF,sub1}}{\dot{q}''_{CHF,sub2}} = \left(\frac{\dot{q}''_{CHF,sub,1}}{\dot{q}''_{CHF,sat}}\right) \Big/ \left(\frac{\dot{q}''_{CHF,sub,2}}{\dot{q}''_{CHF,sat}}\right) \tag{7}$$

results in the data shown on Figure 2.16. A clear dependence on gravity is evident, indicating that the above correlation cannot be used to "correct" the effect of subcooling across gravity levels. An additional term that includes gravity needs to be included. A similar conclusion was made by Di Marco and Grazzi (1999) based on their study of boiling on wires in microgravity.

The time averaged heat flux distribution from each heater in the array is shown on Figure 2.17. The scale has been kept the same for all images to highlight the change in heat transfer with wall superheat and subcooling. Very little heat transfer is associated with the primary bubble, even along the contact line. Much higher heat transfer rates are associated with the rapid growth and coalescence process of the satellite bubbles. A significant amount of the surface

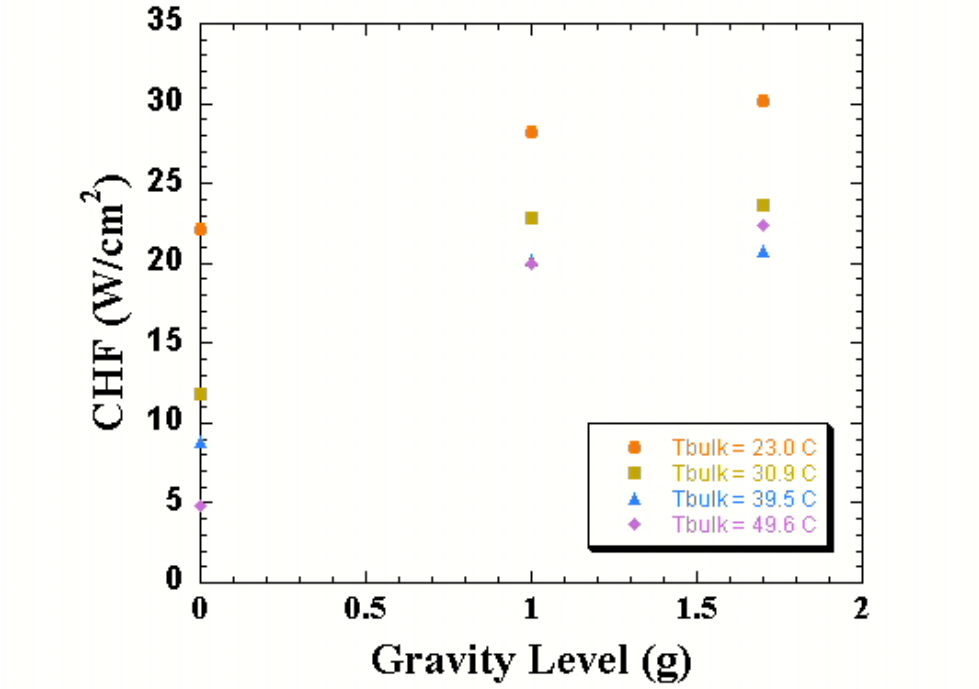

Figure 2.15: Variation in CHF with gravity and subcooling.

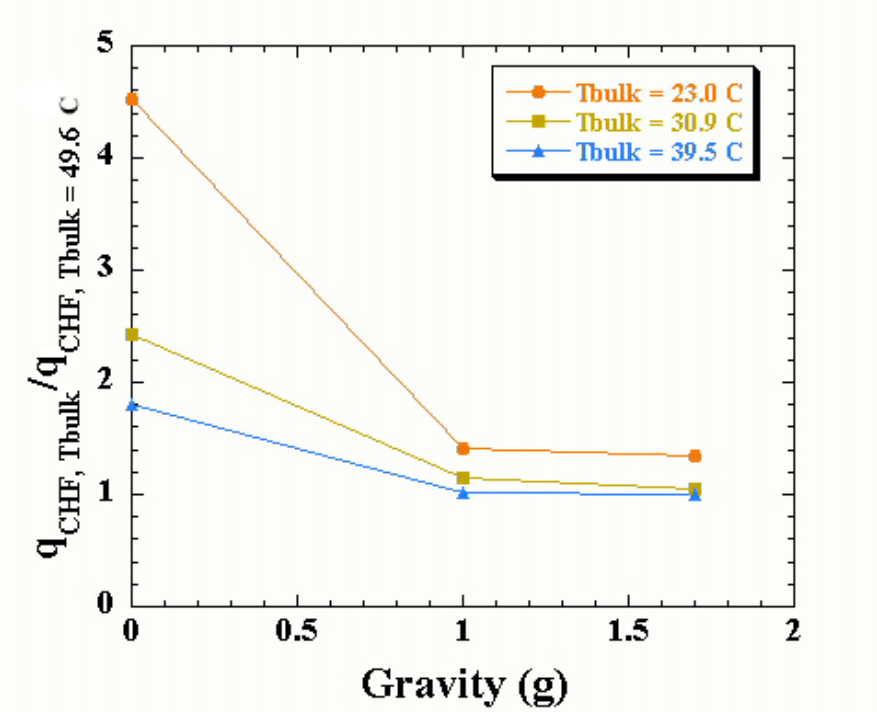

Figure 2.16: Enhancement in CHF normalized on CHF at Tb=49.5 °C.

dries out before CHF. CHF occurs when the dry spot size grows faster than the increase in heat transfer outside the primary bubble. The time averaged heat flux distribution at Tbulk=23.0 °C and a superheat of 31.7 °C under 1 g is shown on Figure 2.18 for comparison. Much more

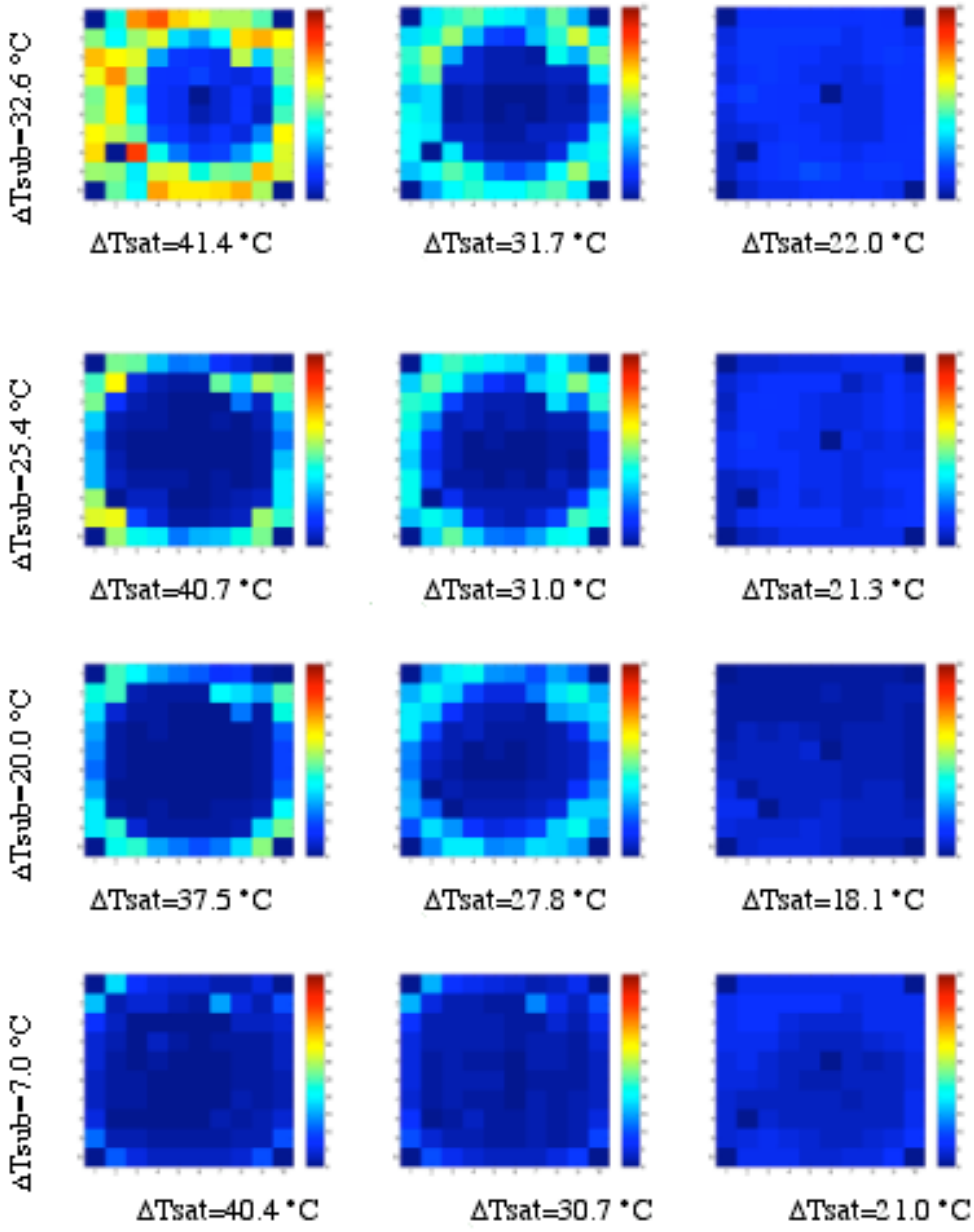

Figure 2.17: Time averaged heat flux from each heater in the array. The color scale ranges from 0-55 W/cm^2.

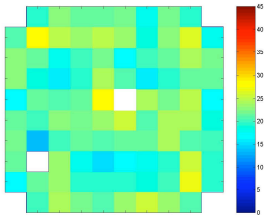

Figure 2.18: Time average heat flux distribution at ΔT_{sub}=33.9 °C, and ΔT_{sat}=30.4 °C in a 1 g environment.

uniform heat transfer across the array is observed since no primary bubble is formed under these conditions.

In order to conditionally sample the heat flux only when boiling occurs on the surface, a *boiling function* was generated from the time-resolved heat flux data. This function is a bimodal signal that is set to HIGH when boiling occurs on the surface, and LOW otherwise. Details of how the boiling function is generated are discussed in Rule and Kim (1999) and Rule (1997). The time average heat flux obtained by sampling the data only when the boiling function is HIGH is referred to as the nucleate boiling heat flux, and is a measure of the heat transfer associated with the satellite bubbles.

One additional step was performed in processing the current results. Because a heater can be partially covered with vapor if the contact line of the primary bubble intersects it, the heat transfer signal may be declared HIGH if the thresholds are set low enough. The heat transfer in this case would be lower than on a heater that was fully wetted with liquid. To minimize the chance that the data from partially wetted heaters is included in the nucleation heat flux, software was written to determine the extent of the dry spot underneath the primary bubble at a given time–only data from those heaters that were at least one heater away in the radial direction from the dry spot were used in the calculation. Also, cases where significant nucleate boiling occurred on fewer than 10 heaters (e.g., T_{bulk}=49.6 °C and T_{sat}=30.7 °C where complete dryout occurred over the array) were discarded since a statistically representative sample was not available.

Boiling curves generated from the nucleate boiling heat flux for microgravity, earth gravity, and high-g environments are compared on Figure 2.19. It is seen that the nucleate boiling heat flux collapses onto a single curve, indicating that the small scale boiling is independent of subcooling and gravity level. This suggests that if one is able to predict the extent of the dry area in microgravity, then one could to predict the microgravity boiling curve from earth or high gravity boiling heat flux data.

Summary of work to date. Our observations to date seem to indicate that microgravity boiling heat transfer is dominated by the formation of a large "primary" bubble on the surface by the coalescence of smaller bubbles. Dryout occurs under the primary bubbles, causing CHF in microgravity to be significantly lower than in earth gravity. The primary bubble also limits the size of the smaller satellite bubbles, causing significant bubble activity and higher heat transfer rates. The primary bubble was also observed to cause nucleation at sites where nucleation would not normally occur, increasing the heat transfer. Preliminary data indicate that subcooling has a strong effect on the size of the primary bubble, and on CHF. Increased CHF were observed for higher liquid subcooling. G-jitter plays an important role as the primary bubble gets larger, and may skew the heat transfer data upward under certain conditions.

Future ground based work. Heat transfer data from heaters even smaller than the ones used here have been obtained, and is currently being reduced. This data was obtained by powering only the inner 64 and 36 heaters. It is thought that below a certain heater size, the coalescence phenomena will cease to occur since nucleation of only a single bubble on the surface will cause dryout of the heater array.

Further experiments are planned to quantify the effect of pressure on boiling behavior. Increased pressure reduces the size of the bubbles, increasing the relative size of the heater array. This will allow the coalescence phenomena to be studied over a wider range of length scales. Increasing the pressure while keeping the bulk fluid at room temperature will also allow boiling data at extremely high levels of subcooling to be obtained since the saturation temperature of the fluid is increased.

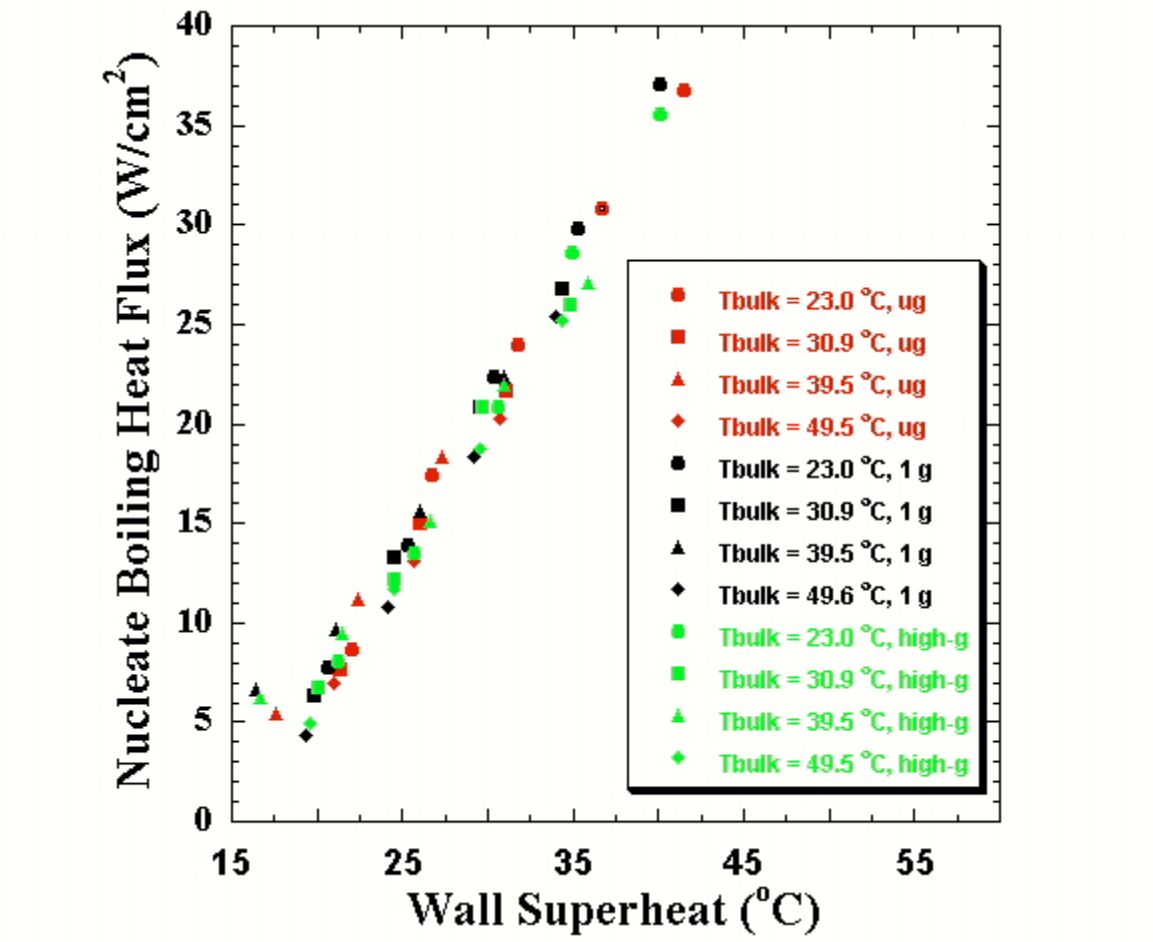

Figure 2.19: Nucleate boiling heat flux.

The effect of sidewalls around the heater array will also be investigated. Sidewalls limit how large the primary bubble can grow, and limit the inflow of liquid to the heater causing dryout to occur at lower superheats.

2.3 MODELS: NUMERICAL AND ANALYTICAL

A substantial portion of the proposed work is to analyze the data and model the boiling process to obtain insight into the boiling heat transfer mechanisms in earth, microgravity, and partial gravity environments. It has been shown by Bae, et al. (1999), Yaddanapuddi and Kim (2000), and Kim, et al. (2000) that the models currently used to predict nucleate boiling heat transfer may be very different from the widely accepted model that microlayer evaporation is the dominant heat transfer mechanism in saturated pool boiling. The large amount of heat transfer that takes place during bubble coalescence is also not explained by any of the models. If similar behavior is observed at high heat flux levels near CHF, then macrolayer and hydrodynamic instability models may also be in error since they assume stationary stems of vapor feeding a large hovering vapor mass.

Numerical techniques have recently been developed that allow simulation of single bubble growth and departure during nucleate boiling. Some examples are the “level set” method of Son and Dhir (1998), and the ALE-FEM method of Fujita and Bai (1998). All of these

models assume axisymmetric bubbles. Tryggvason is currently developing a 3-dimensional, grid adaptive, parallel numerical method to simulate boiling in microgravity–this code is based on the finite difference/front tracking model developed by Unverdi and Tryggvason (1992). The use of one of the two-dimensional codes would be appropriate for the proposed work since the codes are well documented and do not require excessive computation time. Numerical results combined with the experimental results generated in this work would provide unparalleled insight into the boiling process. For example, Bae, et al. (1999a) observed that high wall heat transfer occurred when a small bubble growing underneath a large bubble in earth gravity merged with the large bubble. This case could be numerically modeled using an axisymmetric model of the bubbles to confirm the experimental observations. Results of numerical simulations could also be used to compare with experimentally measured heat fluxes underneath the large, quasi-stationary bubbles that occur in subcooled microgravity boiling. A student is currently developing a code based on the level-set method to simulate the growth of single bubbles.

2.4 KEY ISSUES WHERE KNOWLEDGE IS STILL LACKING

Despite the work to date, it is still not known for certain what the boiling heat transfer mechanisms are in microgravity. In addition to the unknowns regarding boiling in earth gravity, boiling in microgravity seems to be dominated by the behavior of a single primary bubble that forms on the surface of the heater array as a result of the coalescence of smaller "satellite" bubbles. The behavior of the satellite bubbles is thought to be similar to bubbles growing on the surface in earth gravity since they grow quickly and gravity should not play a significant role in their growth. The primary bubble serves to limit the size of the satellite bubbles, and the movement of the primary bubble over the surface can activate normally inactive nucleation sites. Significant portions of the heated surface can be covered with vapor due to the primary bubble, depending on the superheat and subcooling level. Formation of the primary bubble also seems to be the reason CHF in microgravity is a fraction of its value in earth gravity since it causes dryout over a large portion of the surface. These conclusions are tentative, however, since g-jitter complicates the data interpretation. G-jitter can cause the primary bubble to depart or oscillate on the surface, resulting in additional wetting of the surface, artificially elevating the heat transfer levels.

Because the primary bubble seems to play such an important role in microgravity boiling, its characteristics and the parameters influencing it need to be determined. First, can the size of the primary bubble be predicted? The size is determined by many variables, such as nucleation site density, subcooling, gravity level, fluid properties, superheated layer thickness, wall superheat, and surface tension, to name a few. Second, if g-jitter is reduced, then what is the impact of reduced primary bubble motion on heat transfer? Third, what is the effect of heater size on microgravity boiling? Smaller heater sizes are expected to reach CHF at lower wall superheats since dryout under the primary bubble can occur more readily. Fourth, what is the effect of Marangoni convection on bubble growth? Marangoni convection helps hold the primary bubble onto the surface due to the reaction from the "jet" of liquid that is ejected from the top of the bubble into the bulk liquid. It is expected to increase the heat transfer from the wall to the bulk liquid due to thermocapillary motion along the surface of the bubble, and can increase the heat transfer from the wall to the primary bubble and decrease the heat loss from the top of the bubble to the subcooled bulk liquid. The impact of Marangoni convection on 1-g boiling has been found to be negligible (Tong, Bar Cohen, and Simon-1990), but its impact on

microgravity boiling heat transfer is expected to be much larger. The significance of Marangoni convection on microgravity boiling has not been quantified to date.

2.5 OBJECTIVES OF PROPOSED INVESTIGATION

The objective of this effort is to show that boiling curves in microgravity can be obtained from earth gravity data and the size of the primary bubble in microgravity. It is hypothesized that coalescence is the dominant bubble removal mechanisms in microgravity and causes the formation of a large primary bubble. If this bubble is attached to the surface, it causes local dryout to occur, and heat can only be transferred from the surface by the surrounding satellite bubbles. This small-scale boiling behavior is hypothesized to be similar across gravity levels.

Some specific questions we would like to investigate are 1). What does the boiling curve look like in very low g-jitter environments? 2). Does the primary bubble also move on the surface as observed in low g-jitter environments? If not, how does this influence the satellite bubble size? 3). Can the primary bubble size be predicted? What parameters govern the primary bubble size? 4). How does critical heat flux occur in microgravity, and how is it related to the size of the primary bubble? 5). What is the effect of heater size on the primary bubble and how does heater size alter the boiling curves? Boiling curves will be generated for two flat plate heaters of different size at various bulk fluid subcoolings and pressures. Data will be obtained from nucleate boiling through critical heat flux and into transition boiling. The boiling heat transfer mechanisms will be compared to those at lunar, martian, and earth gravity levels. The experimental results will be compared with analytical and numerical models where appropriate.

2.6 FLIGHT EXPERIMENT DESCRIPTION AND CONCEPT

The experimental apparatus will be developed for the ISS based on the ground-based experiment hardware. Additional diagnostics to be incorporated into the flight apparatus are interferometry and a high-speed video camera. A schematic of a modified test cell showing the additional capability is shown on Figure 2.20. Two side view windows allow laser illumination of the test cell along with the capability to visualize the bubbles from the side. Interferometry will be used to obtain temperature contours in the liquid around the bubble. The top and bottom of the chamber hold different size heater arrays. The test section pressure will be monitored and controlled. High-speed video is obtained through the bottom of the heater array. The entire test section will be designed to rotate so that data can be obtained from both heater arrays without disturbing the optics setup. Detailed test setup requirements are discussed in Section 5 below. Because of the heater array's small size, it is possible to significantly reduce the size of the boiling chamber and thus the test fluid inventory. By incorporating a technique to measure the temperature profile within the test fluid coupled with the local heat flux measurements provided by the heater array, it is possible to achieve a better definition of the boiling phenomena.

2.7 ANTICIPATED KNOWLEDGE TO BE GAINED: VALUE AND APPLICATION

The results of this work can be applied towards modeling the behavior of boiling systems in space applications such as cryogenic systems and Rankine cycle based power systems. By developing a relationship between normal gravity and microgravity behavior that relies on the primary bubble size in microgravity, a significant amount of testing can be eliminated since modeling can be based on small-scale normal gravity behavior. The high quality data that can be obtained on the ISS will allow g-jitter free boiling data that will serve as a benchmark for validation of analytical and/or numerical models of the boiling process.

The development of the heater array has enabled us to begin quantifying the contributions to microgravity boiling heat transfer by measuring when and where heat is being transferred from the surface. The use of temperature controlled microscale heaters is especially important in microgravity environments where the formation of a large primary bubble might cause local dryout to occur for a constant heat flux heater array. Long duration CHF and transition boiling studies can be performed without the danger of heater burnout. The transparent nature of the heater array also allows one to overlay the heater power data onto the video images, and can provide significant insight into the position of the phases with respect to evaporation and time. This technique is useful for both microgravity and earth gravity boiling studies.

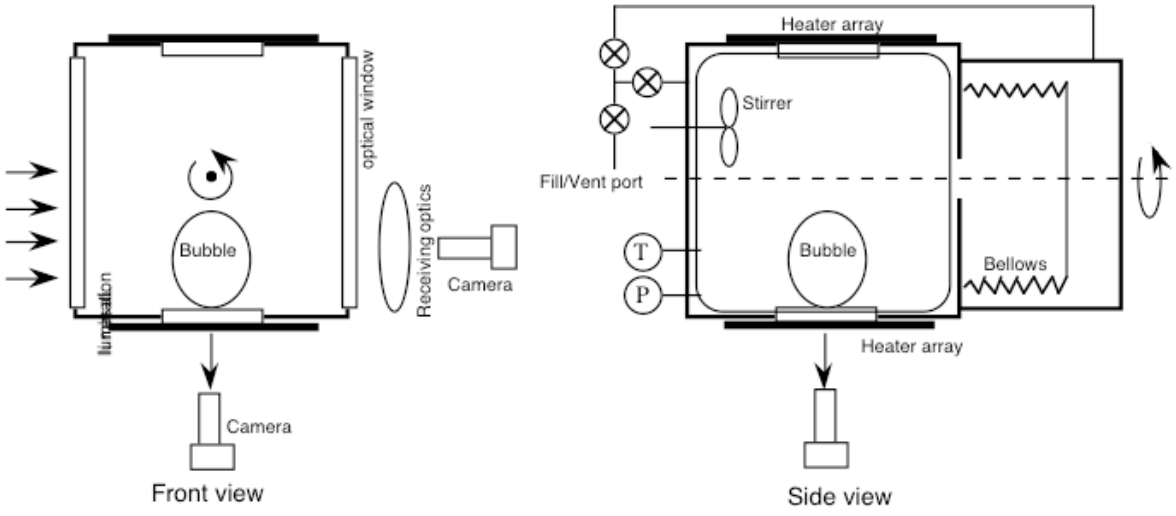

Figure 2.20: Schematic of modified test cell

3.0 JUSTIFICATION FOR CONDUCTING THE EXPERIMENT IN SPACE

Meaningful experiments can be performed in earth gravity and ground-based microgravity facilities such as drop towers and aircraft, as has been shown in Section 2. The long-duration high-quality microgravity of a space-based platform, however, is required if high quality, unambiguous data is desired. The data discussed earlier has shown that g-jitter becomes increasingly important to bubble motion and boiling behavior as the subcooling decreases. Premature bubble departure, bubble motion, and bubble oscillation are some of the effects the residual g-levels on the KC-135 can cause.

3.1 LIMITATIONS OF NORMAL GRAVITY TESTING

Boiling is significantly affected by buoyancy. Experiments in the past have shown that the effect of gravity on boiling processes is not accounted for properly in correlations. For example, the correlation by Rosenhow (1952) for nucleate pool boiling

$$\frac{\dot{q}''}{(T_w - T_{sat})^3} C_{sf}^3 = \frac{\mu c_p{}^3}{h_{fg}^2 \,\mathrm{Pr}^{3s}} \sqrt{\frac{g(\rho_l - \rho_v)}{\sigma}} \tag{8}$$

predicts that the heat flux goes to zero in the absence of gravity, but this is clearly not observed in microgravity. Another commonly used correlation for nucleate pool boiling is given by Cooper (1984)

$$h_{nb} = 55(\dot{q}'')^{0.67} M^{-0.5} P_r^m (-\log_{10} P_r)^{-0.55} \tag{9}$$

where

$$m = 0.12 - 0.2 \log_{10} R_p \tag{10}$$

and P_r=reduced pressure, M=molecular weight, and R_p=rms surface roughness in microns. This correlation does not have any dependence on gravity at all, which is again not consistent with observations.

Also, the models for CHF do not properly account for the effect of gravity, even though they contain a gravity term. Zuber's (1959) correlation

$$\dot{q}''_{\max} = 0.131 \rho_v^{1/2} h_{fg} \sqrt[4]{g(\rho_l - \rho_v)\sigma} \tag{11}$$

which is based on a Helmholtz instability model predicts a vanishing heat transfer as the acceleration approaches zero, as does the similar correlation of Lienhard and Dhir (1973). The macrolayer models of Haramura and Katto (1983) are of similar form, and also predict zero heat transfer.

3.2 LIMITATIONS OF DROP TOWERS AND AIRCRAFT

The high-quality g-level provided by a space-based experiment is needed in these experiments since bubble motion was observed to be sensitive to the residual g-levels in the KC-135 (±0.05 g) when mounted to the aircraft floor. The highly subcooled boiling behavior is not influenced very much by g-jitter since the bubbles are quite small and move actively on the surface. At lower subcooling, however, the primary bubble becomes very large and sensitive to g-jitter. Premature detachment of this large bubble was often observed in the KC-135 tests at lower subcooling. Even when the bubble did not completely detach, it was observed to oscillate back and forth and up and down on the heater surface, causing the contact line to move and the wetted area to change. Free-floating the apparatus was found to provide much lower g-levels, but the test times were found to be severely limited (free-float times of approximately 5 s were typically observed). The formation of a stable primary bubble was not established during this time.

Bubble departure can also be sensitive to the flow within the chamber. For example, Straub, et al. (1997) found that bubbles growing on a small heater (0.26 mm diameter) in the BDPU on IML-2 Space Shuttle mission were occasionally pulled off the heater due to thermocapillary-induced convection currents set up within the chamber under certain conditions. At high subcoolings, a strong thermocapillary motion was set up around the bubble, with the reaction force keeping the bubble on the heater. At low subcoolings (2-3 K), however, the bubble grew to about 1 cm in diameter and the momentum of the flow in towards the bubble due to thermocapillary forces became equal to that away from the bubble caused by the vapor generation, and the bubble departed from the heater. The frequency of bubble departure under these conditions was 0.03 Hz. Clearly, drop towers and aircraft do not provide enough time for such motion to be observed. Drop towers also do not allow enough time for any initial bulk liquid motion to damp out—these convective currents are thought to be responsible for the contradictory early results on microgravity boiling.

The effect of g-jitter on bubble motion can be estimated by calculating the magnitude of bubble oscillation when subjected to a sinusoidally varying g-field. Ishikawa (1994) studied the effect of bubble response to periodic accelerations produced by a piezoelectric actuator within the microgravity environment produced by a TR-IA sounding rocket. Predicted displacements of the bubble agreed well with the measurements. The bubble position vs. time for a bubble subjected to a residual gravity of amplitude g_{osc} and frequency f is given by (Ishikawa–1994)

$$x(t) = \frac{6\pi A}{2\pi f}\sin(2\pi ft) - r^2 A\left[\cos(2\pi ft) - \exp\left(-\frac{6\pi}{r^2}t\right)\right] \tag{12}$$

where

$$A = \frac{2r^2 g_{osc}}{36\pi^2 + r^4(2\pi f)^2} \tag{13}$$

The actual bubble motion is complicated by the presence of a wall, but the above equation can be used to obtain an estimate of the bubble motion. Calculations were carried out for vapor bubbles 0.25 mm to 20 mm in diameter in FC-72. The acceleration level required to produce a displacement of 100 μm (about 40% of an individual heater size) in the bubble motion was determined for varying frequencies. A plot of the acceptable g-levels vs. frequency along with the anticipated ISS environment is shown in Figure 3.1. It is seen that the acceleration environment in the ISS should not affect the bubble motion for frequencies above 0.1 Hz. Also

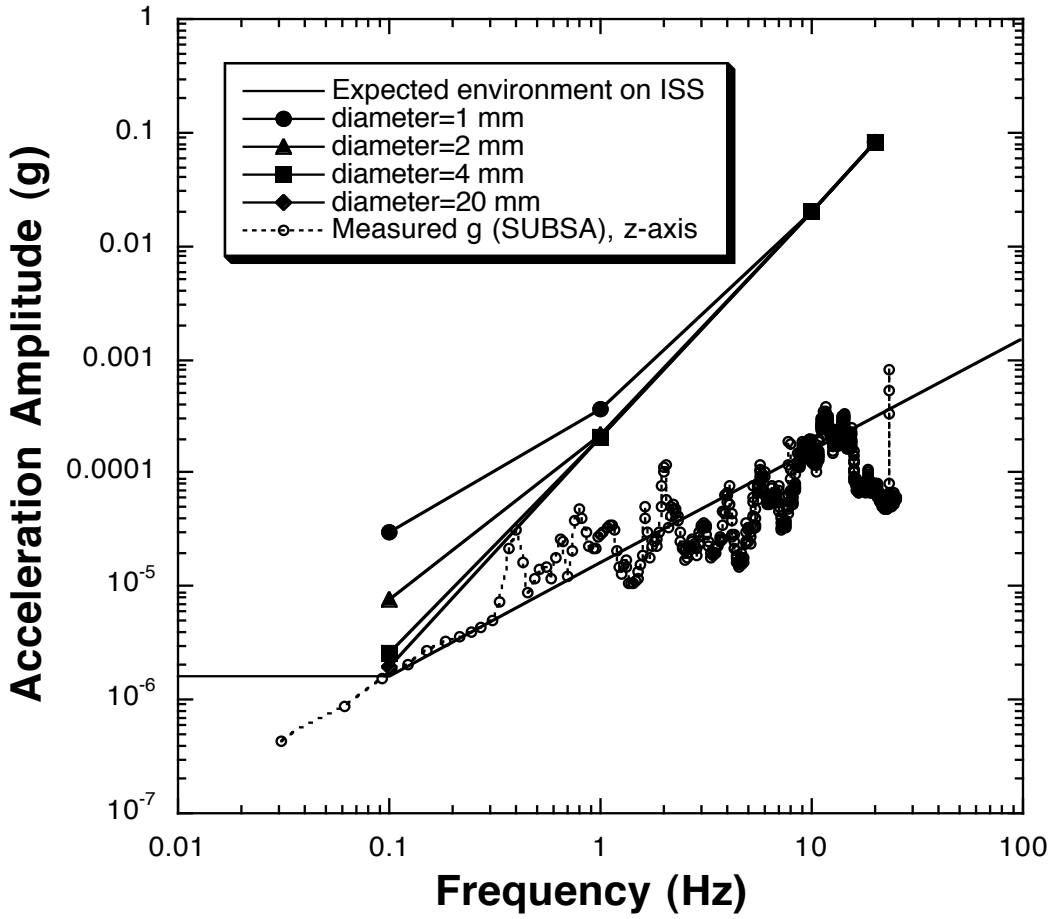

Figure 3.1: Minimum acceptable rms acceleration vs. frequency for various bubble sizes.

plotted on this graph are accelerations in the z-direction measured on the ISS during the SUBSA experiment–they are observed to be similar to the expected environment on the ISS over most of the frequency range, and would be acceptable for MABE. It can be seen that the required accelerations levels are not producible by the KC-135; for a frequency of 1 Hz, the maximum acceptable g-jitter is below 0.001 g, well below the minimum g-jitter on the KC-135. The bubble will not move as much as indicated by Figure 3.1 since surface tension acts to retard bubble motion.

3.3 LIMITATIONS OF MODELING APPROACHES

As mentioned in Section 2.3, numerical simulation of boiling is currently being carried out by various researchers. Limited computational power, however, has enabled simulation of only the simplest of problems to date. For example, Son and Dhir (1998) simulated growth of axisymmetic bubbles growing from a single site, although they have recently been simulating merging of multiple bubbles as well as single bubble departure in a velocity field. Fujita and Bai (1998) simulated single, 2-D bubble growth. Much more powerful computers will be required to simulate the very complex boiling behavior observed in Section 2.2. Also, as computational power increases, validation of the numerical simulations will require high quality, benchmark experimental data.

3.4 NEED FOR ACCOMODATIONS IN THE SPACE STATION

The long duration microgravity in the space station is required to allow sufficient time for the bulk fluid motion to damp out, and to allow the thermal profile near the wall and Marangoni convection around the bubble to develop. An order of magnitude estimate of the time it takes for Marangoni convection to develop can be obtained from Kassemi and Rashidnia (1998), who performed numerical simulations of the developing temperature and flow fields around a gas bubble suddenly injected into an enclosure filled with silicone oil. For cases with Ma>12,000, the flow and temperature fields around the bubble were observed to require approximately 5 s before settling down into a quasi-oscillatory motion with a period of about 2.6 s. Straub, et al. (1997) also observed very slow motion induced in the liquid (R-11) by thermocapillary motion around a small spherical heater during long duration space shuttle experiments. Bubbles that formed on the surface of the heater for subcooling less than 10 °C were observed to depart the surface at a frequency of about 0.03 Hz. Space-based experiments with long microgravity test times would be required to observe such unexpected bubble behavior in the proposed tests.

4.0 EXPERIMENT DETAILS

4.1 FLIGHT EXPERIMENT PLAN AND EXPERIMENT PROCEDURES

The experimental package containing fluid in the test cell and all optics in place will be prepared on the ground. Once on-orbit, the test package will need to be placed within the MSG and connections to the power and vents made.

Once the bulk liquid is brought to the desired subcooling and pressure, a few exploratory runs at low sampling rate (30 Hz for both data and video) will be obtained at various heater temperatures over a long duration (up to 10 minutes) to see if there are long-term changes to the boiling behavior. A test matrix for the exploratory runs is given on Table 4.1. If no long term changes are observed, data from the heater array will be obtained with the wall temperature decreasing from 110 °C down to the saturation temperature of the liquid in 5 °C increments. The liquid will be stirred after data is collected at each wall temperature to ensure the bulk temperature has not changed. It is expected that between 40 s and 120 s worth of data at each wall temperature will be obtained and stored. Side view video data will be obtained throughout the data acquisition time along with interferometry. The speed with which to record using the high-speed camera will depend on the bubble growth rate, and will be an iterative process. Ground based tests have shown that a framing rate of 250 Hz provides adequate temporal resolution.

Although the heater array will be calibrated on the ground before launch, recalibration of the heater array may be necessary in flight. The calibration procedure is discussed in section 5.4.

4.2 TEST MATRIX

A summary of the full test matrix is shown on Table 4.2. The test points are designed so the effects of liquid subcooling, pressure, and heater size on boiling heat transfer can be obtained in an efficient manner. CHF will be reached for a majority of the test conditions, generating a wealth of data regarding the influence liquid subcooling, pressure, and heater size on boiling. At each test condition, the following data will be obtained:

1). The heater temperature will be decreased in 5 °C increments starting from the maximum heater temperature of 110 °C down to just above T_{sat} at each of the test conditions (up to 9 temperatures), enabling boiling curves to be generated from the transition boiling regime through CHF and into nucleate boiling. Wall temperature changes of 5 °C will allow the boiling curve to obtained with good resolution without an excessive number of data runs. All 96 heaters will be active. Between 40 and 120 s worth of data will be obtained at each temperature after the heaters have been set to the desired wall temperature. The duration of data acquisition time depends on the how fast the boiling process reaches equilibrium. It is expected that increased subcooling may require longer data acquisition times since strong Marangoni convection can develop within the test cell and pull bubbles off the heater array, as was seen by Straub, et al. (1997). Data only (no video) at each point from 110 °C down to just above T_{sat} will then be repeated.

2). Data similar to (1) will be obtained but with only the innermost 64 and 36 heaters active, enabling the effect of heater size on boiling to be studied. Data will be taken between 100 °C and T_{sat} in 10 °C increments (5 temperatures with 64 heaters and 5 temperatures with 36 heaters). The data will then be repeated without video. Side and bottom view video images

should be obtained throughout first series of tests. For each test condition, up to nineteen runs with varying combinations of heater temperatures and heaters energized will be run. Fewer runs will be made at the higher pressures since T_{sat} of the fluid increases with pressure.

Heater and video data should be downlinked whenever possible (after every 3 test conditions is desirable) since the heater temperature and test cell pressure can be changed relatively quickly, but the bulk liquid subcooling can take a few hours to stabilize due to the thermal mass of the test package. The test package will need to be reconfigured between Test Conditions No. 9 and 10 to obtain data from the larger heater array. A ground-based automated data reduction system can monitor the quality of the data as it is being obtained, and assist in the decision to repeat the test point or make changes to the test matrix in a timely manner. Some reasons for repeating a run could be 1). setpoints for pressure and temperature not being met, 2). backside cooling not being effective, and 3). extinction of boiling on the surface. The raw voltages across the heater, along with the outputs from temperature and pressure transducers will be converted to engineering units as part of this data reduction program. Synchronization of the heat transfer, video, acceleration, video, and interferometry data is required.

4.3 POSTFLIGHT DATA HANDLING AND ANALYSIS

Postflight recalibration of the heater array will be performed and 1-g data retaken to check for any drift in the heater/electronics. Boiling curves and boiling heat flux curves for all conditions will be computed. Color-coded heat transfer information along with acceleration vectors will be combined with the video data such as shown in Figure 2.9, enabling easy visual correlation of the video and heat transfer data. The video will be used to obtain information on bubble size distributions, and bubble dynamics and behavior.

Side view images of the bubble will be combined with the interferometry data and the acceleration data. The side view images and the interferometry could be combined on a single frame with the bubble image on one half and the interferometry data on the other half, or the interferometry data could be overlayed onto the side view images.

4.4 GROUND TEST PLAN

It is planned to build a preliminary engineering model of the experiment that will be used to test the functionality of the design including the interferometry and high-speed video. This model will be used to obtain preliminary data on the KC-135. Data will be acquired under conditions as similar as possible to flight conditions. Design of the flight hardware will proceed in parallel with these measurements using the MSG simulator if it is available.

Test Conditions No.	Heater Array Size (mm)	Bulk Liquid Temperature (°C)	Pressure (atm), T_{sat} (°C)	No. of Active Heaters	Heater Temperatures (°C)
1	2.7	55	1.0, 56	96	100, 90,80,70
2	2.7	35	1.0, 56	96	100, 90,80,70
3	7	55	1.0, 56	96	100, 90,80,70
4	7	35	1.0, 56	96	100, 90,80,70

Table 4.1: Test matrix for exploratory test runs.

Test Conditions No.	Heater Array Size (mm)	Bulk Liquid Temperature (°C)	Pressure (atm), T_{sat} (°C)	No. of Active Heaters	Heater Temperatures (°C)
1	2.7	40	0.6, 42	96,64, 36	95, 90, 85, 80, 75, 70, 65, 60, 55, 50
2	2.7	55	1.0, 56	96,64, 36	110, 105, 100, 95, 90, 85, 80, 75, 70, 65
3	2.7	60	2.0, 79	96,64, 36	110, 105, 100, 95, 90, 85
4	2.7	35	0.6, 42	96,64, 36	95, 90, 85, 80, 75, 70, 65, 60, 55, 50
5	2.7	45	1.0, 56	96,64, 36	1110, 105, 100, 95, 90, 85, 80, 75, 70, 65
6	2.7	50	2.0, 79	96,64, 36	110, 105, 100, 95, 90, 85
7	2.7	30	0.6, 42	96,64, 36	95, 90, 85, 80, 75, 70, 65, 60, 55, 50
8	2.7	35	1.0, 56	96,64, 36	110, 105, 100, 95, 90, 85, 80, 75, 70, 65
9	2.7	35	2.0, 79	96,64, 36	110, 105, 100, 95, 90, 85
10	7	40	0.6, 42	96,64, 36	95, 90, 85, 80, 75, 70, 65, 60, 55, 50
11	7	55	1.0, 56	96,64, 36	110, 105, 100, 95, 90, 85, 80, 75, 70, 65
12	7	60	2.0, 79	96,64, 36	110, 105, 100, 95, 90, 85
13	7	35	0.6, 42	96,64, 36	95, 90, 85, 80, 75, 70, 65, 60, 55, 50
14	7	45	1.0, 56	96,64, 36	110, 105, 100, 95, 90, 85, 80, 75, 70, 65
15	7	50	2.0, 79	96,64, 36	110, 105, 100, 95, 90, 85
16	7	30	0.6, 42	96,64, 36	95, 90, 85, 80, 75, 70, 65, 60, 55, 50
17	7	35	1.0, 56	96,64, 36	110, 105, 100, 95, 90, 85, 80, 75, 70, 65
18	7	35	2.0, 79	96,64, 36	110, 105, 100, 95, 90, 85

Table 4.2: Full test matrix. Each test will be repeated, but without video.

5.0 EXPERIMENT DETAILS

5.1 SCIENCE REQUIREMENTS SUMMARY TABLE

Section	Experiment parameters	Requirements
5.2	Test fluid	FC-72 (heat transfer fluid - T_{sat} at 1 atm. = 56°C). The fluid shall be distilled until the boiling point is between 56 and 57 °C at 1 atm. The fluid shall be degassed to obtain a target gas concentration of $<1.0x10^{-4}$ moles/mole. The fluid shall be filtered to remove particles larger than 1 μm.
5.3	Experiment Chamber	The minimum chamber size should be 10 cm diameter by 10 cm high. For the 2.7 mm heater, an area 2.5 cm x 2.5 cm centered on it reaching from the heater to the far wall of the chamber shall have no sensors located in it. For the 7 mm heater, an area 4 cm x 4 cm centered on it reaching from the heater to the far wall of the chamber shall have no sensors located in it. Viewing ports for bottom and side viewing. Two heater array attachment ports.
5.4	Heater Arrays	Array sizes of 2.7 and 7 mm, each with 96 heaters with individual heaters 0.27 mm and 0.7 mm in size, respectively. Heater temperature range: 60 to 110 °C, ±2 °C. Enough light transmission thorough the heater arrays to allow imaging Cooled from back side to bring the average array heat transfer to 5 W/cm^2 min over entire range of wall temperatures.
5.5	Bulk Fluid Temperature	Controllable between 30 °C and 60 °C (Tolerance ±1°C). Measurement accuracy of ±1.0 °C. At least six measurement locations within bulk liquid. Pool temperature standard deviation of 1.0 °C.
5.6	System Pressure	0.6–2 atm ± 0.1 atm range, uncertainty of ±0.01 atm. 0.6 atm –5 atm is needed if on-board calibration is to be performed. Pressure set within 2 minutes.
5.7	Acceleration	Measurement resolution of 10^{-6} g. Time stamp to allow correlation with heater and video acquired data. Microgravity environment should be as follows: f<0.01 Hz: 10^{-6} g 0.01 Hz<f<10 Hz: 10^{-4} g 10 Hz<f<100 Hz: 10^{-4}g
5.8	Data Requirements	Heater output voltage acquisition rate□ 500 Hz/heater. System temperature: 1 Hz or greater. Pressure: 20 Hz or greater. Acceleration: 20 Hz or greater. Voltage measurement resolution to 0.01 V.
5.9	Imaging	Bottom view□500 Hz digital video correlated with data acquisition to within 0.5 ms. 512x512 pixels, 10 μm and 30 μm resolution , monochrome, 2000 frames storage min per test. Field of view should be 4 mm x 4 mm for 2.7 mm heater and 1 cm x 1 cm for 7 mm heater. Bottom view: 29.97 Hz, and correlated with data acquisition to within

		30 ms, monochrome, similar field of view as high speed video. Side view□ 29.97 Hz, and correlated with data acquisition to within 30 ms, monochrome. Additional detail regarding imaging is given on Table 5.3 in section 5.9 below
5.10	Astronaut Involvement	Assembly and reconfiguration between 2.7 mm and 7 mm heater array tests.
5.11	Telepresence	At UMD, data and video should be obtained within 8 hours of test completion and next test set. All data from a test is not required–only data from a selectable segment of a test need be downlinked.

Table 5.1□ Summary of science requirements.

5.2 TEST FLUID

The test fluid is FC-72 (C_6F_{14}). This fluid is manufacured by 3M, and is marketed as an electronic fluid. The industrial version of this fluid is also marketed as PF 5060. It is characterized as being non-flammable, chemically non-reactive, and electrically insulating. The boiling point is 56 °C at 1 atm. It is used extensively in wafer fabrication plants to wash and clean wafers prior to dicing and packaging, and is completely compatible with most electronics. FC-72 is chemically inert at temperatures below 200 °C, and poses little risk to personnel under the conditions it is to be used. FC-72 absorbs large amounts of air, about 48% of its volume at 1 atm and 25 °C.

The fluid shall be filtered to remove any particulate matter above 1 □m. It shall also be distilled prior to filling to remove any oils and water that may be present. The distilling process used shall provide a FC-72 product that has a boiling point between 56–57 °C.

The fluids shall be degassed whenever the boiling chamber is opened and the fluid exposed to air. The fluid need not be distilled again. A suggested method for degassing is to repeatedly pull a vacuum on the vapor above the liquid until the pressure above the liquid is equal to the saturation pressure corresponding to the liquid temperature. Any dissolved gases will increase the vapor pressure above this saturation pressure. Henry's law can be used to determine the amount of dissolved gases in the liquid. The dissolved gas concentration C_g (moles gas/mole liquid) in the liquid phase is given by

$$C_g=H(T)P_g \tag{14}$$

where P_g is the partial pressure of the gas above the liquid and H(T) is Henry's constant. For air in FC-72, this has been measured to be $5.4x10^{-5}$ mole/mole-kPa for 31 °C<T<60 °C. P_g can be determined from a measurement of the pressure (P_{tot}) and temperature (T_{sat}) of the gas above the liquid after it has come to equilibrium in a sealed container from the following equation:

$$P_g=P_{tot}-P_{sat}(T_{sat}) \tag{15}$$

where P_{sat} is the saturation pressure of the liquid at the measured temperature T_{sat}. The variation of P_{sat} with T_{sat} is given on Table 5.2. Gas concentrations smaller than $2x10^{-3}$ moles/mole have been shown to have no influence on the boiling behavior (You, et al.–1995)

Tsat (°C)	Psat (atm)
10	0.1438
20	0.2323
30	0.3606
40	0.5404
50	0.7850
60	1.1091
70	1.5288
80	2.0615
90	2.7255
100	3.5410
110	4.5290
120	5.7017

Table 5.2: Saturation temperature vs. pressure for FC-72.

in earth gravity. The fluid should be degassed to a level much lower than this for the space station experiments, however, since residual gas might affect Marangoni convection around the bubble. Because little information is available regarding the importance of gas concentration on the strength of the thermocapillary convection that forms around the bubble in microgravity, it is proposed that the fluid be degassed to as low a level as practical, then document the actual gas concentration. A target concentration of $1x10^{-4}$ moles/mole is suggested. Merte et al. (1998) (who observed Marangoni convection) assumed their fluid (R-113) to be adequately degassed when the measured pressure above the fluid was within 0.025 psia (170 Pa) of the saturation pressure for temperatures measured to within 0.1 °F (0.06 °C). Straub (1997) also observed Marangoni convection during boiling on small, spherical heaters.

A suggested procedure for degassing is to first orient the test cell upside down (bellows on bottom) so that liquid is opposite the vent port. A vacuum pump is then used to pump air out from around the bellows, increasing the volume within which the liquid is contained and causes the liquid to fall away from the vent port. This decreases the pressure above the liquid, and causes gas to come out of solution. Once the pressure has stabilized, the vacuum pump is briefly turned on to vent off the vapor above the liquid. The vapor above the liquid is periodically vented until the desired dissolved gas concentration is reached. The degassing procedure typically takes about 3 days. If the boiling chamber is opened to atmosphere for any reason, then the fluid shall be degassed again.

5.3 EXPERIMENT CHAMBER

The experiment chamber should be large enough not to interfere with the bubble growth. The maximum size of the primary bubble is determined strongly by the subcooling. At equilibrium, the vapor added to the bubble at its base will be balanced by the condensation of vapor through the bubble cap. At lower subcoolings, the bubble condenses less vapor at the top and the primary bubble increases in size. Based on the measurements performed to date in the KC-135, the bubble can grow to up to 1 cm in diameter on the smaller heater array (2.7 mm heater array size) for a subcooling of 5 °C and heater temperatures between 85 °C and 100 °C. If the bubble scales as the heater size under similar conditions, then the bubble can grow to be as large as 2.6 cm in diameter for the larger heater array (7 mm heater array size). The minimum size of the test chamber is 10 cm diameter and 10 cm high. For the 2.7 mm heater, an area 2.5 cm x 2.5 cm centered

on it reaching from the heater to the far wall of the chamber shall have no sensors located in it. For the 7 mm heater, an area 4 cm x 4 cm centered on it reaching from the heater to the far wall of the chamber shall have no sensors located in it.

The chamber should have viewing ports for the side-view images. It should be able accommodate two heater arrays. There should also be a means to fill the liquid, vent gas and provide pressure control. A bellows can be used for the pressure control and degassing of the fluid (see section 5.2).

The experiment chamber should be designed so that data can be obtained from either heater arrays with a minimum of astronaut involvement. This could include repositioning the chamber, optics, cameras, and command/control/data cables. One possible configuration for this chamber was shown on Figure 2.20.

5.4 HEATER ARRAYS

Local heat flux measurement and temperature control can be performed using an array of platinum resistance heater elements deposited on a quartz wafer in a serpentine pattern. The heater should allow about 50% light transmission so that pictures of boiling on the heater can be obtained through the substrate. The heater array is currently made of platinum deposited onto a quartz substrate in a serpentine pattern. Each elements is 0.27 mm x 0.27 mm in size, with a nominal resistance of 1000 Ω, and a nominal temperature coefficient of resistance of 0.002 °C^{-1}. Ninety-six individual heaters are arranged in a square array about 2.7 mm on a side. It is desired to manufacture a similar heater array about 7 mm in size with individual heaters 0.7 mm in size so that measurements can be made over a larger area. The temperature of the microscale heaters are set using an array of electronic feedback loops (Figure 2.2) as discussed in section 2.1.

The instantaneous power dissipated in each heater can be obtained by measuring the voltage across it vs. time. Because all the heaters in the array are at a set temperature, heat conduction between adjacent heaters can be measured and subtracted from the total power supplied to the heater element, enabling the heat transfer from each individual heater to the fluid to be determined. The maximum voltage across the heater is about 10 V. For a 0.27 mm, 1000 Ω heater, the maximum heat flux that can be dissipated is 137 W/cm^2. For a 0.7 mm, 250 Ω heater, the maximum heat flux is 82 W/cm^2. Typical uncertainties in heat flux after correction for substrate conduction have been found to be about 2 W/cm^2 (Bae, et al., 1999).

Calibration of the microscale heater array can be performed by placing the array in a constant temperature environment and increasing the position of a digital potentiometer (R_1 in Figure 2.2) in the circuit controlling a particular heater until the circuit begins to regulate–this is indicated by an increase in the output voltage (V_{out} in Figure 2.2). This can be repeated for all the heaters in the array at a given temperature, and for temperatures between 60–110 °C in 5 °C increments. Calibration of the heater array should repeatable within 2 digital potentiometer positions for all heaters.

Range, accuracy, and response rate. For the resistor values indicated, a heater of nominally 1000 Ω resistance can be varied over a 350 Ω range. Since the heaters have a temperature coefficient of resistance of nominally 0.002 °C^{-1}, the temperature of the heaters can be varied by approximately 175 °C. For typical resistance values used in the circuit of Figure 2.2, one step in the digital potentiometer corresponds to about 0.34 °C in heater temperature, which represents the minimum uncertainty in heater temperature. If the heater temperature can be controlled to within ±3 positions, then the uncertainty in heater temperature is ±1 °C. The

calibration uncertainty should be approximately ±0.3 °C. The feedback loop/heater combination was measured to have a frequency response of 15 kHz.

Cooling of heater array. The heater array should be cooled from the back of the wafer. This cooling is necessary to prevent individual heaters from shutting off at low heat transfer values (such as occurs when the primary bubble covers the heater). It shifts the heat transfer data for each heater array upward a fixed amount. The amount of the shift can be measured during data acquisition, and subtracted to find the actual heat transfer from the heater surface to the liquid. We have found that an air jet at ambient temperature with a flow rate of 230 cc/s, flowing through a 1.59 mm diameter nozzle, placed ~0.7 cm from center of heater array, and offset by about 24° from the normal provides sufficient cooling of the heater over the entire range of wall temperatures and bulk subcoolings.

5.5 BULK FLUID TEMPERATURE

The temperature of the bulk fluid may vary from 20 °C up to 110 °C during heater calibration, and needs to be controlled to within ±1.0 °C. It is expected to be varied from 30 °C up to 60 °C during testing.

Location and number of sensors. Six temperature sensors should be placed above and around the heater array to measure bulk liquid temperature above the heater (similar to those used for Merte's experiment). Two sensors should be placed in the vicinity each heater array, perhaps 1 cm beyond the edge of the array and 2 cm above it, to measure the local temperature, and four should be placed at other locations within the boiling chamber to measure the temperature uniformity. The sensors should not interfere with the growth of the bubble.

Range, accuracy, and response rate. The temperature sensors should be able to measure temperatures between 15 °C and 120 °C with an accuracy of 1.0 °C. The response rate can be as low as 2 Hz.

5.6 SYSTEM PRESSURE

System pressure needs to be controlled for two reasons. First, we wish to investigate the influence of pressure on boiling behavior. Second, the system pressure needs to be increased during calibration to prevent boiling of the fluid at the maximum heater temperature.

Range, accuracy, and response rate. The chamber pressure will be varied between 0.6-2 atm during data acquisition. If an in-situ calibration system is developed, then the chamber pressure can be as high as 5 atm. The pressure within the test chamber should be held to within ±0.01 atm of the set pressure (this corresponds to about ±0.3 °C change in saturation temperature), and the set pressure should be reached within 2 minutes. The response rate of the pressure transducer can be as low as 2 Hz.

5.7 ACCELERATION□ MAGNITUDE, DIRECTION, AND FREQUENCY

Acceleration data and roll rates for all three axes should be acquired and time stamped (by a third party, if necessary). This acceleration data can then be synchronized with the acquired test data and recorded throughout the data acquisition period. Acceleration and roll rates should be resolved to within10^{-6} g and 1°/min, respectively. The minimum sampling rate for acceleration is 10 Hz. The quasi-steady acceleration levels (frequencies below 0.01 Hz) should be kept below 10^{-6} g. The vibratory components should be kept to below 10^{-4} g for $0.01<f<10$ Hz throughout the experiment. The vertical axis of the test chamber should be aligned

with one of the principal axes of the accelerometer. In the event the acceleration exceeds the required levels during the data acquisition, data acquisition should continue.

5.8 DATA REQUIREMENTS

The voltage across each of the 96 heaters in the array should be sampled at 500 Hz for up to 120 s. The length of data acquisition time will depend on how long it takes for "steady" boiling to be established. This will be determined during flight, but is expected from preliminary KC-135 measurements to be at least 30 s. A few exploratory runs for long times (minutes) at low data sampling rate and using the 30 Hz video will be used to determine how long it takes for "steady state" to be established. The data taken during the flight should be archived onto disk as well as downloaded to ground periodically. It is desired to download all of the data after each test run, including the video images within three hours after data acquisition at a given test point and before acquiring data at the next test point.

The bulk temperature will be held constant during data acquisition, and should change slowly if at all. It should be sampled at 1 Hz throughout the data acquisition duration. The bulk pressure may change due to boiling activity on the surface, and should be sampled at 20 Hz or greater. The acceleration data needs to be sampled 20 Hz or greater, since the maximum frequency of interest is about 10 Hz. The video data (bottom and side views along with the interferometry) should also be downloaded through the video link periodically.

All heater voltages will be in the 0–10 V range, and should have a measurement accuracy of 0.01V. Temperature, pressure, and acceleration signals should be sampled to obtain the required resolution.

5.9 IMAGING

Imaging shall be principally in the visible spectrum and be a combination of high-speed and normal frame rate video that will focus on the bubble nucleation, growth, movement and detachment. A summary of the imaging requirements is given in Table 5.3.

Bottom view camera. High speed digital video is required to observe the bubble motion from below the heater array. A Phantom V4.0 monochrome digital video camera from Vision Research (www.visiblesolutions.com) or equivalent would be adequate for this view. The high speed digital video will be used to acquire images at speeds up to 500 fps. The ability to store 2000 frames should provide adequate recording time. The high-speed video can be processed in flight and selected data should be downlinked within 8 hours of acquisition. A time stamp and run number superimposed on every frame of the video is desirable. This camera must be able to image an area about 20% larger than the heater arrays to image any boiling that might occur on the substrate surrounding the heaters. The resolution of the camera should be 512 x 512 pixels. The depth of field should be at least 1 mm, but as large as possible consistent with the lens used and available lighting.

Bottom view images using a standard 29.97 Hz video camera is also required to document the boiling behavior throughout each test. The field of view is the same as for the high-speed camera. It would be preferable to obtain these images using the NTSC output of the high speed digital camera if it is available. This video will be post-processed to obtain de-interlaced and interpolated images at 59.94 fps. A shutter speed of 1/1000 s or faster is desired to minimize blur due to bubble movement.

Side view camera. The side-view video will acquire images at a standard 29.97 Hz and recorded on videotape. The side-view video will be post-processed to obtain de-interlaced and

Camera	#1		#2		#3	
Type	High-speed–Bottom		Standard Rate–Bottom		Standard Rate–Side	
View	Bottom 2.7 mm Array	Bottom 7.0 mm Array	Bottom 2.7 mm Array	Bottom 7.0 mm Array	Side 2.7 mm Array	Side 7.0 mm Array
Speed (Hz)	500	500	29.97	29.97	29.97	29.97
Pixels	512 x 512	512 x 512	640 x 480	640 x 480	640 x 480	640 x 480
Resolution (μm)	40	60	40	60	180	180
Storage per test	2000 frames	2000 frames	120 s	120 s	120 s	120 s
Object Plane	Array leads	Array leads	Array leads	Array leads	Array Center	Array Center
Image Center	Array Center	Array Center	Array Center	Array Center	Array Center	Array Center
Field of View (mm)	4.0 x 4.0	10.0 x 10.0	4.0 x 4.0	10.0 x 10.0	40 x 40 (W x H)	40 x 40 (W x H)
Depth of Field (mm)	> 1	> 1	> 1	> 1	Best Effort	Best Effort
Shutter Speed(Hz)	> 1000	> 1000	> 1000	> 1000	> 1000	> 1000
Time correlation with electronic data	< 0.5 ms	< 0.5 ms	< 30 ms	< 30 ms	< 30 ms	< 30 ms

Table 5.3: Summary of imaging requirements.

interpolated images at 59.94 fps. This camera (side view) should be able to view the heater array and about 4 cm above it. The camera should be positioned to obtain a clear view of the heater array. The depth of field should be as large as possible consistent with the lens used and available lighting. A shutter speed of 1/1000 s or faster is desired to minimize blur due to bubble movement.

Illumination. Enough light should be provided to illuminate and provide sufficient contrast at the bubble interface for the bottom view. It has been found using the sounding rocket test rig that a bank of 100 white LEDs (Nichia NSPW500BS), each emitting 5.6 candles provide sufficient illumination to backlight the bubbles using the Phantom V4.0 camera and an Infinity KC lens at 500 fps and a shutter speed of 1/1000 s. Advantages of this lighting arrangement include low energy consumption (12 W), low heat dissipation, microsecond response (important for synchronization of the side-view video and the data), and small form factor. A similar system would be adequate for this experiment.

Synchronization with data. All images need to be synchronized with the heater data. The high-speed video camera has the capability of being externally triggered using the same signal used to trigger data acquisition.

5.10 ASTRONAUT INVOLVEMENT AND EXPERIMENT ACTIVATION

The astronaut involvement should be minimal. Their task may include the following:

1). Installation into MSG.
2). Changing wiring connections from one heater to another and/or digital I/O.
3). Reconfiguration between 2.7 mm and 7 mm heater array tests.
4). Changing out video tape and hard drives occasionally.
5). Focusing cameras only if needed.

6). Activating and deactivating the experiment.
7). Removal of experiment from MSG after operations are complete.

5.11 TELEPRESENCE

The investigator team requires the use of telepresence to set and monitor the experimental conditions, particularly the bulk fluid temperature and pressure, the power input into the microscale heaters, and video. During the actual data acquisition, no monitoring is necessary; however, data and selected video should be downloaded to the investigator team so we can verify heater performance before the next set of tests is conducted. To minimize the amount of telemetry data, it is proposed to download all of the heater array, pressure and bulk liquid temperature, but only frames 0, 400, 800, 1200, 1600, and 2000 from the high speed images. No side or bottom view video data obtained at 29.97 Hz need to be downloaded. All processing of data will be performed on the ground.

5.12 POST FLIGHT DATA DELIVERABLES

The collected data for the space-flight experiment shall be in the following format:

1. For each test conducted, there should be a data file (ASCII format), indicating the following:
   - A. A unique test number (to be used to identify corresponding detailed scientific data and flow visualization data).
   - B. liquid absolute pressure (MPa)
   - C. bulk liquid section temperature (°C)
   - F. data acquisition rates (Hz)
   - G. video imaging rates (Hz)
   - H. mission elapsed time at the start of the test (to match the acceleration measurements, visualization data, and microscale heater data).
2. Flow visualization data recorded in the following format:
   - A. S-VHS tapes (NTSC format)
   - B. Digital image files
3. Instrumented heater array data in voltages using IEEE binary format.
4. Calibration data to convert the microscale heater array test section data from voltages into heat fluxes (W/cm^2), and interferometry data (°C).
5. Acceleration data vs. mission elapsed time.

5.13 SUCCESS CRITERIA

There are two levels of success criteria defined: minimum and significant.

Minimum Success

- Complete Test Matrix for at least two subcooling levels (pressure and temperature of bulk liquid) for one heater array.
- Record at least 80 channels of heater array power level data
- Record view through heater array at 250 Hz
- Record pressure and temperature of bulk liquid
- Record residual acceleration levels

Significant Success

- Meets Criteria for Minimally Successful□
- Complete Test Matrix for at all subcooling levels for one heater array
- Record at least 90 channels of heater array data
- Record side view of bubble growth and temperature field images

6.0 REFERENCES

Bae S., Kim M., Kim J. (1999) "Improved Technique To Measure Time- And Space-Resolved Heat Transfer Under Single Bubbles During Saturated Pool Boiling Of FC-72," *Experimental Heat Transfer,* Vol. 12, No. 3, pp 265-278,.

Bae, S.W., Kim, J., Mullen, J.D., and Kim, M.H., (1999a) "Wall Heat Flux Variation Underneath Bubbles During Pool Boiling of FC-72", Journal of Heat Transfer, Heat Transfer Gallery, Vol. 121.

Bar-Cohen, A. and Simon, T.W. (1988), "Wall superheat excursions in the boiling incipience of dielectric fluids", Heat Transfer Engineering, Vol. 9, No. 3, 1988.

Clark, J.A., 1968, "Gravic and Agravic Effects in Cryogenic Heat Transfer," Advances in Cryogenic Heat Transfer 87, Vol. 64, pp. 93–102.

Cooper, M.G. (1984) "Saturation nucleate, pool boiling–a simple correlation", Institution of Chemical Engineers Symposium Series, Vol. 86, pp. 785-792.

Dhir, V.K., Qui, D.M., Ramanujapu, N, and Hasan, M.M. (1998) "Investigation of nucleate boiling mechanisms under microgravity conditions", Proceedings of the Fourth Microgravity Fluid Physics and Transport Phenomena Conference, Cleveland, OH.

Di Marco, P. and Grassi, W., (1999) "About the Scaling of Critical Heat Flux with Gravity Acceleration in Pool Boiling", XVII UIT National Heat Transfer Conference, Ferrara, June 30-July 2.

Fritz, W. (1935) "Berechnungen des Maximalvolumens von Dampfblasen", Phys. Z., Vol. 36, pp. 379-384.

Fujita Y, Bai Q, "Critical Heat Flux Of Binary Mixtures In Pool Boiling And Its Correlation In Terms Of Marangoni Number" *International Journal Of Refrigeration-Revue Internationale Du Froid*, Vol. 20: pp 616-622, 1997.

Fujita, Y. and Bai, Q. (1998), "Numerical simulation of the growth for an isolated bubble in nucleate boiling", Proceedings of the 11th International Heat Transfer Conference, Kyongju, Korea, Vol. 2, pp. 437-442.

Ishikawa, M., Nakamura, T., Yoda, S., Samejima, H., and Goshozono, T. (1994) "Responsive motion of bubbles to periodic g-jitter", Microgravity Science and Technology, Vol. VII, No. 2.

Han, C.Y. and Griffith, P. (1965) , "The mechanism of heat transfer in nucleate pool boiling–Part I", Int. J. of Heat and Mass Transfer, Vol. 8, pp. 887.

Haramura, Y. and Katto, Y.A. (1983) "A new hydrodynamic model of critical heat flux applicable widely to both pool and forced convection boiling on submerged bodies in saturated liquids", Int. J. of Heat and Mass Transfer, Vol. 26, pp. 389-399.

Kassemi, M. and Rashidnia, N. (1998) "Bubble dynamics on a heated surface", Proceedings of the Fourth Microgravity Fluid Physics and Transport Phenomena Conference, Cleveland, OH.

Keshock, E. G. and Siegel, R., "Effects of reduced gravity on nucleate boiling bubble dynamics in water," *NASA-TM-X-57461,* 1963.

Kim, J. and Benton, J.F., "Subcooled Pool Boiling Heat Transfer in Earth Gravity and Microgravity", Proceedings of the 2001 National Heat Transfer Conference, Anaheim, CA, June, 2001.

Kim, J., Benton, J.F., and Kucner, R. (2000), "Subcooled Pool Boiling Heat Transfer Mechanisms in Microgravity: Terrier-Improved Orion Sounding Rocket Experiment", NASA CR-2000-210570.

Kim, J., Demiray, F., and Yaddanapudi, N. (2000) "Saturated Pool Boiling Mechanisms During Single Bubble Heat Transfer: Comparison at Two Temperatures", Proceedings of the 2000 ASME IMECE, Orlando, FL.

Kim, J., Yaddanapuddi, N., and Mullen, J.D., "Heat Transfer Behavior on Small Horizontal Heaters During Saturated Pool Boiling of FC-72 in Microgravity", to appear in Microgravity Science and Application, 2001.

Koffman and Plesset (1983) "Experimental Observations of the Microlayer in Vapor Bubble Growth on a Heated Surface", Journal of Heat Transfer, Vol. 105, pp. 625-632.

Lee, H.S. and Merte, H. (1998) "Pool boiling phenomena in microgravity", Proceedings of the 11th International Heat Transfer Conference, Kyongju, Korea, Vol. 2, pp. 395-400.

Lienhard, J.H. and Dhir, V.K. (1973) "Hydrodynamic prediction of peak pool-boiling heat fluxes from finite bodies", J. Heat Transfer, ASME Serial C, Vol. 95, pp. 152-158.

Merte, H., Lee, H.S., and Keller, R.B. (1998) "Dryout and rewetting in the Pool Boiling Experiment Flown on STS-72 (PBE-IIB) and STS-77 (PBE-IIA).

Mikic, B.B. and Rosenhow, W.M. (1969), "Bubble growth rates in non-uniform temperature field", Prog. in Heat and Mass Transfer, Vol. II, pp. 283-292.

Nakayama, A. and Kano, M. (1992), "Liquid motion in saturated-pool nucleate boiling by interfering bubbles", Heat Transfer-Japanese Research, pp. 805-815.

Ohta, H., Kawaji, M.., Azuma, H., Inoue, K., Kawasaki, K, Okada, S., Yoda, S., and Nakamura, T. (1998) "Heat Transfer in nucleate pool boiling under microgravity condition", Proceedings of the 11th International Heat Transfer Conference, Kyongju, Korea, Vol. 2, pp. 401-406.

Ohta, H., Kawaji, M., Azuma, H., Kawasaki, K, Tamaoki, H., Ohta, K, Takada, T., Okada, S., Yoda, S., and Nakamura, T. (1997) "TR-1A Rocket Experiment on Nucleate Boiling Heat Transfer Under Microgravity", ASME-MEMS, HTD-Vol. 354, pp. 249-256.

Rosenhow, W.M. (1952) "A Method of Correlating Heat Transfer Data for Surface Boiling of Liquids", Transactions of the ASME, Vol. 74, p. 969.

Rule, T. (1997) "Design, Construction, and Qualification of a Microscale Heater Array for use in Boiling Heat Transfer", Thesis for Master of Science in Mechanical Engineering, Washington State University.

Rule and Kim, J., "Heat Transfer Behavior on Small Horizontal Heaters During Pool Boiling of FC-72", Journal of Heat Transfer, Vol. 121, No. 2, May, 1999, pp. 386-393.

Rule, T.D., Kim, J., Quine, R.W., Kalkur, T.S., and Chung, J.N. (1999), "Measurements of Spatially and Temporally Resolved Heat Transfer Coefficients in Subcooled Pool Boiling", *Convective Flow and Pool Boiling*, Edited by Lehner, M. and Mayinger, F., Taylor and Francis.

Siegel, R., 1967, "Effects of Reduced Gravity on Heat Transfer," Advances in Heat Transfer, Vol. 4, Academic Press, New York/ London, pp. 143–228.

Siegel, R., and Keshock, E. G., 1964, " Effects of Reduced Gravity on Nucleate Boiling Bubble Dynamics in Saturated Water," Journal A.I.Ch.E. 4, Vol. 10, pp. 509– 517.

Son, G. and Dhir, V.K. (1998) "Numerical simulation of a single bubble during partial nucleate boiling on a horizontal surface", Proceedings of the 11th International Heat Transfer Conference, Kyongju, Korea, Vol. 2, pp. 533-538.

Steinbichler, M., Micko, S., and Straub, J. (1998) "Nucleate boiling heat transfer on a small hemispherical heater and a wire under microgravity", Proceedings of the 11th International Heat Transfer Conference, Kyongju, Korea, Vol. 2, pp. 539-544.

Straub, J., Picker, G., Winter, J., and Zell, M. (1997) "Effective Cooling of Electronic Components by Boiling Phase Transition in Microgravity", Acta Astronautica, Vol. 40, No. 2-8, pp. 119-127.

Tong W., Bar Cohen A., Simon T.W., You S.M., "Contact-Angle Effects On Boiling Incipience Of Highly-Wetting Liquids," *International Journal Of Heat And Mass Transfer,* Vol. 33: 91-103 1990.

Tong W., Bar Cohen A., and Simon, T.W. (1990) "Thermal Transport Mechanisms in Nucleate Pool Boiling of Highly-Wetting Liquids", Proceedings of the Ninth International Heat Transfer Conference, Jerusalem, I-BO-05, pp. 27-32.

Ulucakli M.E., Merte H, "Nucleate Boiling With High Gravity And Large Subcooling," *Journal Of Heat Transfer-Transactions Of The ASME,* Vol. 112: pp. 451-457, May 1990.

Unverdi S. O., Tryggvason G., "A Front-Tracking Method For Viscous, Incompressible, Multi-Fluid Flows," *Journal Of Computational Physics*, Vol. 100: pp. 25-37 1992.

Vogel B., Straub J., "Influence Of Marangoni Convection On Pool Boiling," *Fizika Nizkikh Temperatur*, Vol. 16: pp 532-535, 1990.

Xu, J.J. and Kawaji, M. (1998) "Study of liquid-solid contact in transition boiling regime under reduced and normal gravity conditions", Proceedings of the 11th International Heat Transfer Conference, Kyongju, Korea, Vol. 2, pp. 419-424.

Yaddanapudi, N., and Kim, J., (2001) "Single Bubble Heat Transfer in Saturated Pool Boiling of FC-72", Accepted for publication in Multiphase Science and Technology.

You, Simon, Bar-Cohen, and Hong, (1995) Effect of dissolved gas content on pool boiling of a highly wetting fluid□, Journal of Heat Transfer, Vol. 117, pp. 687-692.

Zell M, Straub J, Vogel B., "Pool Boiling Under Microgravity," *Physicochemical Hydrodynamics,* Vol. 11: pp 813-823, 1989.

Zell, M., Straub, J., and Vogel, B., 1990, "Heat Transfer in Pool Boiling under Microgravity," Soviet Journal of Low Temperature Physics 16(5), pp. 323–324.

Zell, M., Straub, J., and Weinzierl, A., 1984, "Nucleate Pool Boiling in Subcooled Liquid under Microgravity – Results of Texus Experimental Investigations," Proceedings of the 5th European Symposium on Material Sciences under Microgravity, Schloss Elmau, ESA SP-222, pp. 327–333.

Zuber, N. (1959) "Hydrodynamic aspects of boiling heat transfer", AEC Report AECU-4439, Physics and Mathematics.

7.0 APPENDIX–EXPERIMENT DATA MANAGEMENT PLAN (EDMP)

Microheater Array Boiling Experiment: (MABE)

1.0 CONTACT INFORMATION

1.1 ***Principal Investigator***

Prof. Jungho Kim
Department of Mechanical Engineering
University of Maryland
College Park, MD 20742
301/405-5437
FAX: 301/314-9477
kimjh@eng.umd.edu

1.2 ***Project Scientist***

John McQuillen
NASA Glenn Research Center
21000 Brookpark Road
Cleveland, OH 44135
216/433-2876
216/433-8050
j.mcquillen@lerc.nasa.gov

1.3 EDMP Author

John McQuillen
NASA Glenn Research Center
21000 Brookpark Road
Cleveland, OH 44135
216/433-2876
216/433-8050
j.mcquillen@lerc.nasa.gov

1.4 ***Archive Center Technical Contact***

Nancy Hall
NASA Glenn Research Center
21000 Brookpark Rd.
Cleveland, OH 44135
216/433-5643
216/433-8050
nancy.hall@lerc.nasa.gov

2.0 EXPERIMENT DESCRIPTION

2.1 ***Experiment Name:*** Microheater Array Boiling Experiment (MABE)

2.2 ***Mission***

2.3 ***Purpose*** To detemine local heat transfer coefficients and mechanism for pool boiling as a function of the gravity level for nucleate and transition boiling regimes.

2.4 ***Method*** The experiment uses an array of microheaters to measure the local heat transfer on the surface during boiling. Each heater is on the order of the bubble departure size in normal gravity, but significantly smaller than the bubble departure size in reduced gravity. These heaters are individually controlled to operate at a constant temperature, simplifying the data analysis since the substrate heat conduction can be easily quantified. It also allows one to operate at CHF and into the transition boiling region without danger of heater burnout.

2.5 ***Facility Used*** Microgravity Science Glovebox aboard ISS, US Lab Module

2.6 ***General Experiment Summary***

2.7 ***Summary of Results and Data***

2.8 ***Keywords***

2.8.1 ***Discipline:*** Microgravity

2.8.2 ***Subdiscipline:*** Fluids

2.8.3 ***Parameter Group*** Heat Transfer

2.8.4 ***Parameter*** Boiling

2.8.5 ***General Keywords*** Two-phase, bubble, nucleate boiling

3.0 PROCESSING AND ANALYSIS DESCRIPTION

3.1 ***Measurement Techniques***

3.1.1 Local surface heat flux and temperature measurements are provided by an array of ninety-six platinum resistance heaters deposited on a quartz wafer. Each individual heater is about 0.26 mm x 0.26 mm in size, has a nominal resistance of 1000 ohms and a nominal temperature coefficient of resistance of 0.002 $°C^{-1}$.

3.1.2 High speed digital video provides imaging of the bubble through the heater array. Standard video provides a side view.

3.1.3 Point Diffraction Interferometry is used to measure temperature profiles around the vapor bubble

3.2 ***Analysis Techniques Performed***

4.0 ARCHIVING AND ACCESSIBILITY

4.1 ***Data Archive Center*** NASA Glenn Research Center

4.2 ***Inventory of Data to be Archived***

4.2.1 ***Video Tape*** Hi-8 Videocassette tape, 120 minutes record time, 9 tapes total from side view camera

4.2.2 ***Film*** None

4.2.3 ***Digital Data*** The following types of data files should be obtained for each test point

- Readme file containing the following
  - A unique test number (to be used to identify corresponding detailed scientific data and flow visualization data).
  - liquid absolute pressure (MPa)
  - bulk liquid section temperature (°C)
  - data acquisition rates (Hz)
  - video imaging rates (Hz)
  - mission elapsed time at the start of the test (to match the acceleration measurements
- Digital image files
  - High speed video camera
  - inteferometry data
- Instrumented data in voltages using IEEE binary format.
- Calibration data to convert the microscale heater array test section data from voltages into heat fluxes (W/cm^2), and interferometry data (°C).
- Acceleration data vs. mission elapsed time

4.2.4 ***Samples:*** None

4.2.5 ***Other***

4.2.6 ***Publications/Reports/etc***

4.2.7 ***Related Ground Based Experiment Data***

4.2.8 Data Not Archived

4.3 ***Data Accessibility and Availability***

4.4 ***Policies for Proprietary Data***

Rev. Date: 24 April, 2003